Deep–Sea Research II 208 (2023) 105269

Contents lists available at ScienceDirect

Deep-Sea Research Part II

journal homepage: www.elsevier.com/locate/dsr2

Iron cycling during the decline of a South Georgia diatom bloom

Joanna Ainsworth [a,*], Alex J. Poulton [b], Maeve C. Lohan [a], Mark C. Stinchcombe [c], Alastair J.M. Lough [a], C. Mark Moore [a]

[a] School of Ocean and Earth Science, National Oceanography Centre Southampton, University of Southampton, Southampton, SO14 3ZH, UK
[b] The Lyell Centre for Earth and Marine Science and Technology, Heriot-Watt University, Edinburgh, EH14 4AS, UK
[c] National Oceanography Centre, Southampton, SO14 3ZH, UK

ARTICLE INFO

Handling Editor: J Aristegui

Keywords:
Iron
Phytoplankton
Remineralisation
Mesopelagic
South Georgia bloom

ABSTRACT

The Southern Ocean is the largest high nutrient low chlorophyll (HNLC) oceanic region, where iron limits phytoplankton growth and productivity and ultimately influences the Biological Carbon Pump (BCP). Natural exceptions to the HNLC regime occur where island wakes cause iron to be mixed into surface waters from sediments, enabling large, prolonged phytoplankton blooms and increased carbon drawdown. Interactions between iron and phytoplankton are reciprocal in blooms: with plankton regulating the (re)cycling of iron through cellular uptake and remineralisation. The depth of iron remineralisation then influences either re-supply to the surface mixed layer biota or sequestration into deeper waters. Water column trace metal observations and shipboard experiments, using bioassays and radioisotope (^{55}Fe, ^{32}Si, ^{14}C) cycling, were undertaken to investigate surface mixed layer phytoplankton iron limitation, iron uptake, and mesopelagic iron remineralisation relative to carbon and silica within the November 2017 bloom downstream of South Georgia. Surface phytoplankton residing in the iron depleted mixed layer were iron limited throughout the four-week sampling period. Experiments designed to investigate particulate water column (re)cycling revealed limited iron remineralisation from freshly produced upper ocean particles. The main pathway of iron transfer from particulates into the dissolved phase was through rapid (<2 d) release of extra-cellular adsorbed iron, which, if occurring *in situ*, could contribute to observed higher sub-surface dissolved Fe concentrations. This was accompanied by a small loss of cellular carbon, likely through respiration of the fixed ^{14}C, and limited dissolution of particulate ^{32}Si to dissolved ^{32}Si. Decoupling of the remineralisation length scales for Fe, C and Si, with Fe having the fastest turnover, is thus likely in the upper mesopelagic zone beneath the bloom.

1. Introduction

The Southern Ocean forms an important component of the global biogeochemical cycles of carbon (C) and macronutrients, being the most extensive and biogeochemically important of the so-called high nutrient low chlorophyll (HNLC) regions (Chisholm and Morel, 1991). Nutrient rich waters in the Southern Ocean could support large blooms of phytoplankton if limiting factors such as iron (Fe), low light availability and low temperatures were alleviated (Boyd, 2002), converting dissolved inorganic carbon (DIC) into particulate organic carbon at the base of the marine food web. The carbon that is fixed by phytoplankton maybe directly or indirectly respired by bacteria in the surface mixed layer of the ocean (Ducklow et al., 1993; Cole et al., 1988; Boyd et al., 2019), respired by higher trophic levels or transported as sinking particles to the deep ocean, generating long-term storage via the Biological Carbon Pump (BCP) (Eppley and Peterson, 1979). The high macronutrient levels of the Southern Ocean are due to strong upwelling of nutrient rich deep waters (Pollard et al., 2006) accompanied by low phytoplankton production due in part to Fe limitation (Martin, 1990). Enhanced primary production and drawdown of atmospheric CO_2 can thus occur in Fe enriched Southern Ocean waters (Martin, 1990; Blain et al., 2007; Pollard et al., 2009).

Phytoplankton need to access bioavailable Fe for key cellular processes, including nitrate and nitrite reduction, chlorophyll synthesis, and the electron transport chains of respiration and photosynthesis (Twining and Baines, 2013; Reuter, 1988). The availability of Fe therefore influences the C and nitrogen cycles. However, Fe has low solubility in oxygenated waters, which limits concentrations and hence its availability (Raiswell and Canfield, 2012). Iron is also particle reactive and rapidly scavenged from the water column onto particles (Goldberg,

* Corresponding author.
E-mail address: jja1u16@soton.ac.uk (J. Ainsworth).

https://doi.org/10.1016/j.dsr2.2023.105269
Received 26 May 2021; Received in revised form 23 September 2022; Accepted 19 January 2023
Available online 20 January 2023

1954), which can sink through the euphotic zone into mesopelagic waters (100–1000 m), with the possibility of being remineralised and recycled at all stages (Boyd et al., 2017). Both factors make Fe a scarce resource for surface mixed layer ocean biota in the modern oxic ocean. Dissolved unchelated inorganic concentrations, the most readily available form of Fe to phytoplankton (Morel et al., 2008), can be in the picomolar range (Johnson et al., 1997), while organic Fe-binding ligands increase Fe solubility (Kuma et al., 1996) allowing dissolved Fe to remain in the water column at nanomolar concentrations, a proportion of which can also be bioavailable to marine phytoplankton (Maldonado et al., 2005; Rijkenberg et al., 2008; Hassler et al., 2020). These low concentrations of bioavailable Fe exert notable controls on global phytoplankton productivity, species composition and therefore ecosystem structure and the carbon cycle (Chisholm and Morel, 1991; Boyd and Ellwood, 2010).

The interactions between Fe and plankton are reciprocal: the plankton regulate the distribution, chemical speciation, and cycling of Fe through cellular uptake and remineralisation processes (Sunda, 2012). The depth of Fe remineralisation thus controls either its resupply to the surface mixed layer phytoplankton (shallow recycling of Fe) or sequestration into deep mesopelagic waters, with eventual upwelling supporting further primary production (Boyd et al., 2017). Dissolved Fe (dFe: <0.2 μm) therefore often displays nutrient like depth profiles due to its key biological role in the oceans; removal in surface mixed layer waters by biological uptake and increased concentrations at depth from the breakdown of cells and remineralisation processes, moderated by the extent of scavenging (Boyd and Ellwood, 2010).

Iron sources to biota in the Southern Ocean can be in the form of new Fe (additions to the upper ocean Fe inventory) or recycled Fe (turnover of the inventory) (Boyd and Ellwood, 2010). Most new Fe supply to the surface mixed layer of the Southern Ocean comes in the form of upwelling of Fe rich deep waters (Boyd and Ellwood, 2010; Tagliabue et al., 2014). Other sources of Fe can originate from coastal or shallow sediment resuspension, ice melt, dust deposition, hydrothermal activity, vertical diffusive flux and island wakes (Boyd and Ellwood, 2010). Within the Southern Ocean, natural exceptions to the low productivity HNLC regions are found downstream of continental shelves and islands such as the Kerguelen Plateau, Crozet Islands and South Georgia, where large phytoplankton blooms have been observed (Blain et al., 2007; Pollard et al., 2007; Korb et al., 2008; Nielsdottir et al., 2012). It is generally accepted that enhanced Fe supply to surface mixed layer waters in these systems predominately occurs from sediment sources being mixed into the surface on the shallower shelf regions through internal waves and other mixing processes (Blain et al., 2007; Schlosser et al., 2018). Iron not immediately used to produce new biomass locally can then be transported downstream via lateral advection, alleviating the limitation of phytoplankton further afield (Boyd et al., 2007: Korb et al., 2008; Nielsdottir et al., 2012; Schlosser et al., 2018).

The South Georgia region lies within the Antarctic Zone of the Antarctic Circumpolar Current, to the south of the Polar Front (Orsi et al., 1995) and is characterised by high biomass and productivity of phytoplankton (Atkinson et al., 2001). The high productivity is widespread, occurring far downstream off the shelf and possibly extending northwards to the Polar Front (Atkinson et al., 2001). High phytoplankton concentrations (>6 mg chlorophyll-*a* m^{-3}) within the central bloom may be linked to enhanced supply of Fe, though silicic acid concentrations may also be limiting to diatoms in this region (Atkinson et al., 2001). The phytoplankton growth season is long, with blooms (>2 mg chlorophyll-*a* m^{-3}) persisting for 4–5 months (Atkinson et al., 2001; Robinson et al., 2016). The blooms are fertilised by Fe from South Georgia sediments or from elsewhere within the basin (Antarctic peninsula or ice melt) (Nielsdottir et al., 2012; Robinson et al., 2016; Schlosser et al., 2018) and are dominated by large diatoms (Atkinson et al., 2001; Korb et al., 2008, 2010).

Iron cycling can thus exert notable control on production and ultimately the efficiency of the BCP, including in naturally Fe fertilised regions of the Southern Ocean such as downstream of South Georgia (de Baar et al., 1995) or the Crozet Islands (Pollard et al., 2009). Surface mixed layer ocean interactions between trace metal and carbon cycles have thus received great attention, however, less work has been performed on the (de-) coupling of these cycles within the mesopelagic zone (the so-called 'twilight zone' at ~100–1000 m) (Boyd et al., 2017; Tagliabue et al., 2019). Iron is remineralised differently to both C and macronutrients such as nitrogen and silica (Si). Differential cycling in the twilight zone could ultimately influence atmospheric CO_2 through multiple feedback mechanisms, including influences on the depth of C, Si and Fe remineralisation and the corresponding potential for different nutrients to become limiting to surface mixed layer production (especially Fe and Si in the Southern Ocean) either locally or through interactions with the large-scale oceanic circulation, remotely and/or globally (Lamborg et al., 2008).

Previous work has investigated the cycling of radioisotope labelled surface ocean particulate material in the surface mixed layer with one (Fe) (Boyd et al., 2010) or two (C and Si) (Bidle and Azam, 1999) elements being investigated for their relative remineralisation rates, presumably by bacteria. In the case of Boyd et al. (2010), rapid algal Fe mobilisation by bacteria collected in the mixed layer was observed over a 72-h incubation period, however in these experiments it was not possible to discriminate between the pools of intra- and extra-cellular (adsorbed) algal Fe.

To elucidate controls on upper ocean Fe cycling, as well as the potential for vertical transport and the cycling of Fe relative to C and Si in the upper mesopelagic (100–300 m), we performed trace metal sampling and incubation experiments during the 2017 South Georgia diatom bloom (Sanders et al., this issue). Depth profiles of Fe and other comparative trace metals (manganese (Mn), zinc (Zn), nickel (Ni), copper (Cu) and cobalt (Co)) provide a time series of initial conditions to compliment the experimental work. Experimental enrichment combined with observations of phytoplankton biomass and physiology were used to determine the surface (20–30 m) phytoplankton response to Fe. Remineralisation experiments were performed to assess the uptake and relative movement of Fe, C and Si between particulate and dissolved phases when the phytoplankton were resuspended in mesopelagic (110 m) water. These remineralisation experiments aimed to investigate the potential role mesopelagic processes play in the (re)cycling of major nutrients and trace metals. The work was undertaken as part of the COMICS (Controls over Ocean Mesopelagic Interior Carbon Storage) project. COMICS aimed to further understand the processes that contribute to mesopelagic remineralisation, to expand the knowledge of the C cycle and to investigate how this will interact with global climate change in the future (Sanders et al., 2016).

2. Material and methods

2.1. Sampling

A series of trace metal sampling and experimental work was performed on board the *RRS Discovery* (cruise DY086, 12th November to 19th December, 2017) at a single site in the South Atlantic sector of the Southern Ocean northwest of South Georgia, during the austral spring of 2017 (Sanders et al., this issue). We performed 3 sampling cycles near the British Antarctic Survey (BAS) long term sampling station P3 (occupation periods hereafter named P3A, P3B and P3C) from 15th November to 15th December, 2017. P3 is located off the shelf in >3000 m water depth (Fig. 1). The study site was located within the region of higher chlorophyll-*a* concentrations representing the South Georgia bloom (Fig. 1). General oceanographic parameters for the station occupations are presented in Tables 1 and S1. Water samples were collected through deployment of a Titanium framed trace metal Conductivity, Temperature and Depth instrument (TM CTD) fitted with 24 × 10 L OTE bottles that have been modified for trace metal work with epoxy coated external springs, coating of stainless ferrules and fitting of

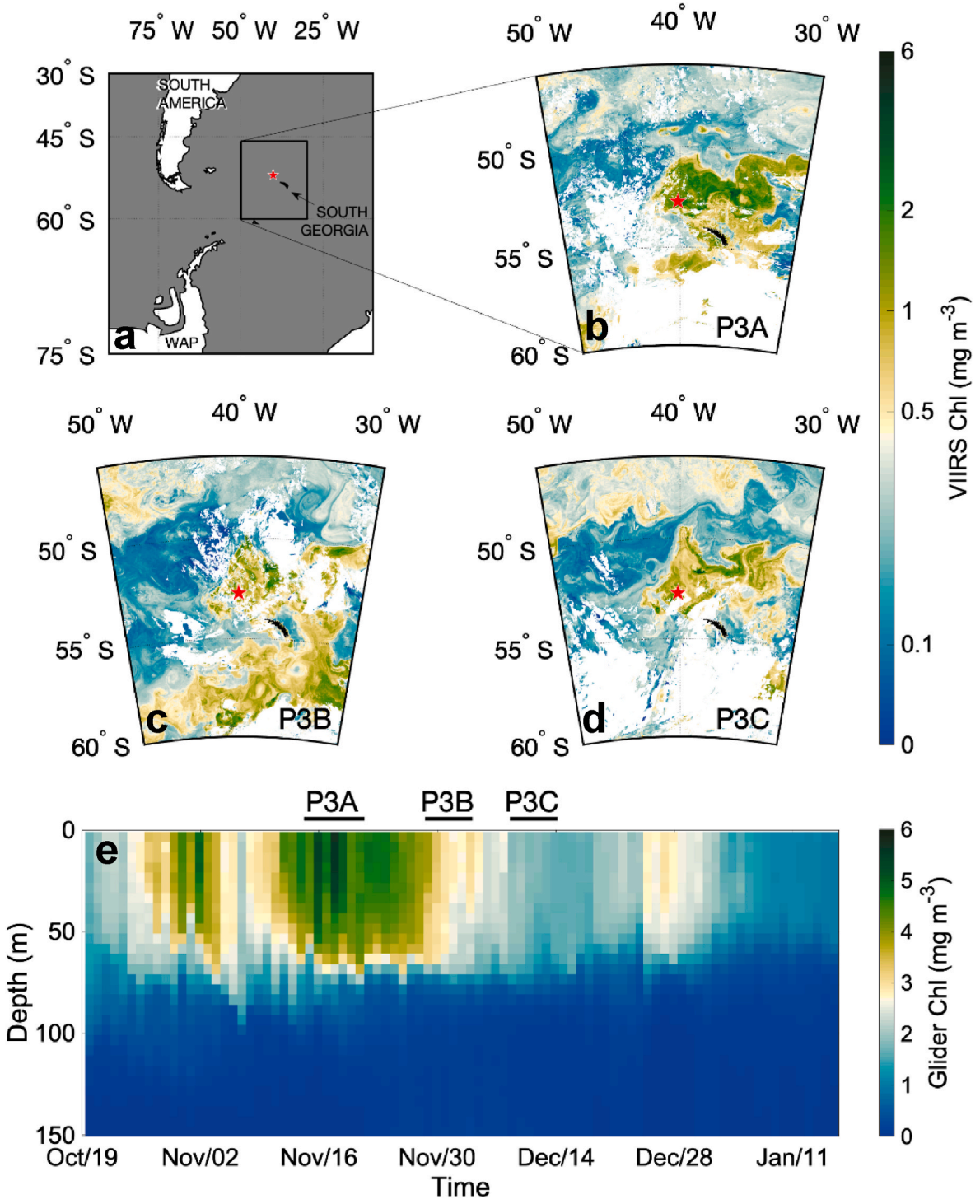

Fig. 1. Sampling locations and chlorophyll-a concentrations around South Georgia during 15th November to 15th December, 2017. (a) Expanded location of sampling site P3 (red star) relative to South Georgia, South America and the West Antarctic Peninsula (WAP). (b, c and d) Location of sampling station over the three periods indicated by the red star (P3A, P3B and P3C, respectively) relative to South Georgia (black landmass) and satellite-derived chlorophyll-a concentrations (week-long composites from VIIRS (Visible Infrared Imaging Radiometer Suite), white shading represents insufficient data). (e) Depth distribution over time of calibrated chlorophyll-fluorescence from glider data (GOCART, Carvalho et al., this issue), indicating the three temporal sampling periods.

PTFE taps. Trace metal clean protocols were employed in the deployment and subsequent sampling of the TM CTD (Cutter et al., 2010). Samples for trace metals and experiments were collected from the TM CTD whilst samples for Chlorophyll-*a*, particulate organic carbon (POC) and biogenic silica ($bSiO_2$) were collected from stainless steel (SS) CTD deployments, macronutrients were collected from both the TM and SS CTDs.

2.2. Iron addition bioassay experiments

To determine whether the surface phytoplankton communities were Fe limited, four (once at P3A, twice at P3B and once at P3C) surface community Fe limitation experiments were performed using protocols similar to those employed by Moore et al. (2007a&b) and Nielsdottir et al. (2012). Water was collected from the TM CTD, with OTE bottles

transferred into a class-1000 clean air laboratory for sampling. For each experiment, 6 sub-samples were collected from OTE bottles fired in the upper mixed layer (20–30 m nominal depth) into acid-washed 250 mL polycarbonate bottles. Of these, 3 bottles were left as un-amended controls and 3 were amended with 2 nM Fe additions (50 μl of 10 μM $FeCl_3$ in 0.024 M HCl). Unamended controls and Fe amended bottles were incubated for up to 5 days in a dedicated temperature controlled refrigerated container laboratory (see Richier et al., 2014) maintained close to *in situ* temperatures at 2 ± 1 °C under a daily light cycle (16:8 h light:dark) with a total daily irradiance dose of 21.2 mol quanta m^{-2} d^{-1} (i.e. ~60% daily surface irradiance). Bottles were removed to a clean laboratory where subsamples (100 mL) were collected for active chlorophyll fluorescence measurements and determination of chlorophyll-*a* (50 mL; see section 2.4) at 2 days and 4–5 days within each incubation. Active chlorophyll fluorescence measurements on the incubated samples were performed with a prototype 'single turnover fluorescence of enclosed samples (STAFES)' instrument (designed by Chelsea Technologies (UK) Ltd.) and were analysed to recover the apparent photochemical quantum efficiency (F_v/F_m) using protocols similar to those used previously (Moore et al., 2007a; Nielsdottir et al., 2012).

2.3. Remineralisation experiments

We adapted the protocols of Bidle and Azam (1999) and Boyd et al. (2010) to investigate the mesopelagic remineralisation potential of fresh surface organic material. Three experiments were performed to follow the partitioning between size fractionated particulate and dissolved phases, with sampling at three time points (T1 after 1–2 days, T2 after 3–4 days and T3 after 5–8 days incubation post resuspension) during the incubation of surface material in mesopelagic water. The uptake rates of Fe, C and Si by the surface phytoplankton/microbial community were measured through separate radio-labelling (^{14}C, ^{55}Fe, ^{32}Si) of surface communities and parallel incubations (Fig. 2). The large size fraction (>5 μm) from these labelled microbial communities were then harvested via gravity filtration and particles re-suspended to determine the subsequent remineralisation potential of this material by the mesopelagic microbial community, through determination of the fractional (re-) distribution of each radioisotope/element within dissolved and particulate phases (Boyd et al., 2010).

Stage 1: Near surface samples (18–30 m) were collected in TM CTD OTE bottles and transferred into triplicate acid-washed 125 mL Nalgene polycarbonate bottles for each isotope (^{14}C, ^{32}Si and ^{55}Fe). To encourage the active uptake of isotopes through the generation of fresh labelled organic material, all samples were amended with 2 nM of unlabelled Fe (50 μl of 10 μM $FeCl_3$ in 0.024 M HCl). Sufficient Fe was added to all bottles (i.e., those including ^{55}Fe and those not) in order that Fe limitation was relieved and hence enhanced fresh biomass was produced. Within 30 min of unlabelled Fe addition, the samples were then spiked with the radioisotopes; ^{55}Fe, 2 kBq in 10% spa HCl (0.02 kBq/mL; 1.85 nM total addition); ^{14}C as sodium bicarbonate, ~74 kBq (7.4 kBq/mL); and ^{32}Si as orthosilicic acid, 3 kBq (0.05 kBq/mL). After spike addition, each bottle was placed in the incubation container under the same light and temperature environment as the Fe addition bioassay experiments (section 2.2) for 48 h. Sub-samples of 10 mL were then harvested through filtration (<100 kPa) onto 0.2 μm and 5 μm polycarbonate filters to measure total community and >5 μm community uptake, respectively. Additional 1 mL samples were taken to determine the total activities for the 3 isotopes added. An accumulation of measurement error of between −2% and +15% was recorded between the amount of radioisotope used for resuspension and the total amount measured at each time point (a positive value is the measured total value being greater than the resuspended total).

To differentiate between intracellular uptake and adsorption of ^{55}Fe onto external particulate surfaces, subsets of filtered particulates were washed at the end of the sample filtration with a buffered Ti-EDTA-citrate solution which scavenges adsorbed ^{55}Fe (Hudson and Morel, 1989). Once all subsamples had been removed, incubation bottles were rinsed once with seawater before a further sample was taken to determine the ^{55}Fe adsorbed to the walls of the sample bottles by adding 5 mL of 10% HCl, rinsing, and then taking a 1 mL subsample of this HCl rinse. All filters, filtrates and acid rinses were placed in 6 mL Ultima Gold scintillation cocktail before being counted on a liquid scintillation counter (PerkinElmer TriCarb 3180 TR/SL).

Stage 2: At the termination of stage 1, the remainder of the samples (~100 mL) not used for T0 measurements (see above) were harvested by gravity filtration through a 47 mm, 5 μm polycarbonate filter (Fig. 2). Particulate material was then rinsed twice with filtered (0.2 μm) mesopelagic water from TM CTD OTE bottles before being washed off the filter and resuspended into 30 mL of trace metal clean water collected from OTE bottles in the mesopelagic (110 m). A 1/3 split of each resuspension per time point was further diluted into a total of 125 mL of whole (i.e., unfiltered, unamended) mesopelagic water (collected via TM CTD OTE bottles from 110 m) for 3 subsequent harvesting time steps for each isotope. This was repeated to create triplicates for each isotope at each time point. The particulate material (>5 μm) from stage 1 that was resuspended into mesopelagic water then becomes the total activity carried over into stage 2 of the experiment for measurement and subsequent partitioning analysis (Fig. 2).

All stage 2 samples were incubated in the dark at *in situ* mesopelagic temperatures within a temperature controlled container for a minimum of 24 h, to allow time for bacterial colonisation (Bidle and Azam, 1999), and processed at 3 time steps to determine the resultant activity partitioning in each phase of remineralisation. Quantification of activity within each phase (size fractionated particulate, adsorbed, dissolved and wall wash) used methods similar to the end-point measurements at the termination of stage 1 (Fig. 2b). Additionally, determination of dissolved inorganic carbon ($DI^{14}C$) was undertaken through a modification of the Micro-Diffusion Technique (Paasche and Brutak, 1994; Balch et al., 2000) whereby 1 mL of filtrate subsamples were acidified (1 mL, 50% HCl) in gas-tight containers with a CO_2 trap (Whatman™ filter soaked with 200 μL β-phenylethylamine, Sigma-Aldrich). The activity on the β-phenylethylamine soaked filters and filtrates was determined by liquid scintillation counting and are assumed to correspond to the partitioning of the dissolved C pool into respired C (filters) and dissolved organic carbon (filtrates), respectively.

From these measured values a dissolved fraction can be calculated as the difference between the total sample and the >0.2 μm particulates. A smaller particulate fraction of <5 μm can be calculated as the difference between the measured particulate size fractions (Fig. 2b, see also Supplementary Material Data calculations and validation).

2.4. Ancillary measurements

Samples for chlorophyll-*a* analysis (50–250 mL) were filtered onto 25 mm diameter Whatman™ glass fibre GF/F filters for total chlorophyll-*a* concentration or sequentially through 47 mm diameter polycarbonate 10 μm, 2 μm and 0.2 μm polycarbonate filters for size-fractionated chlorophyll-*a*. In all cases, chlorophyll-*a* was extracted in 6 mL of 90% acetone over 18–20 h at 4 °C in a fridge in the dark. Chlorophyll-*a* fluorescence was measured on a Turner Designs Trilogy™ fluorometer using a non-acidification module calibrated with solid and pure chlorophyll-*a* standards (Sigma-Aldrich, UK).

Inorganic macronutrient concentration of nitrate (NO_3) and silicic acid ($Si(OH)_4$) were sampled in 15 mL centrifuge tubes rinsed three times with seawater from the same sampled Niskin bottle. Analysis was generally within 24 h of the samples being taken. Analysis was on a QuAAtro 39 segmented flow autoanalyzer according to methods provided from *SEAL Analytical UK Ltd*.

Biogenic Silica ($bSiO_2$) samples (500 mL) were filtered onto polycarbonate filters (0.8 μm pore size, Whatman™) and briefly rinsed with pH adjusted MilliQ water (~pH 8.5) to remove any salt residue. Filters were placed into 15 mL corning tubes, dried (overnight at 40–50 °C)

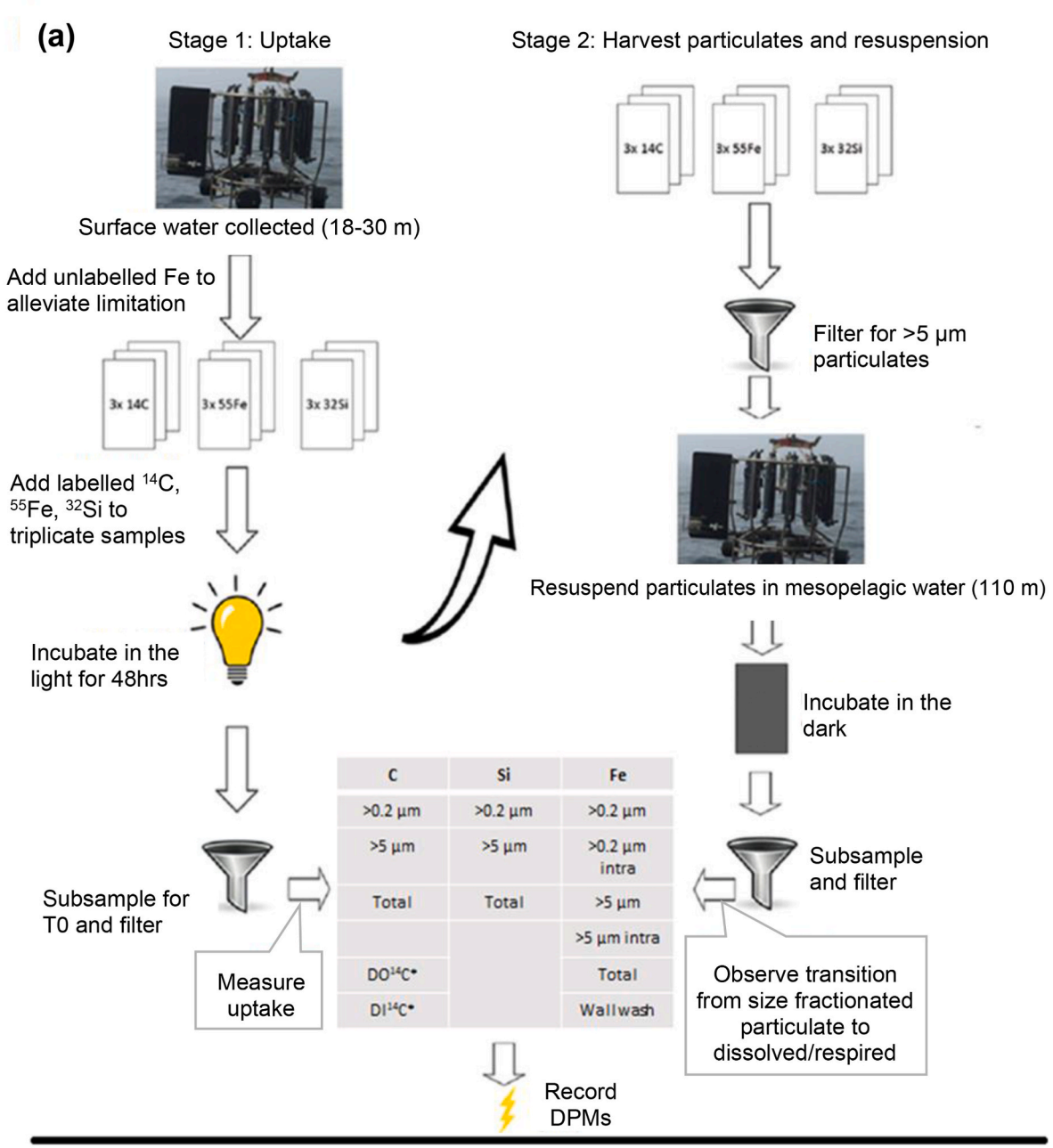

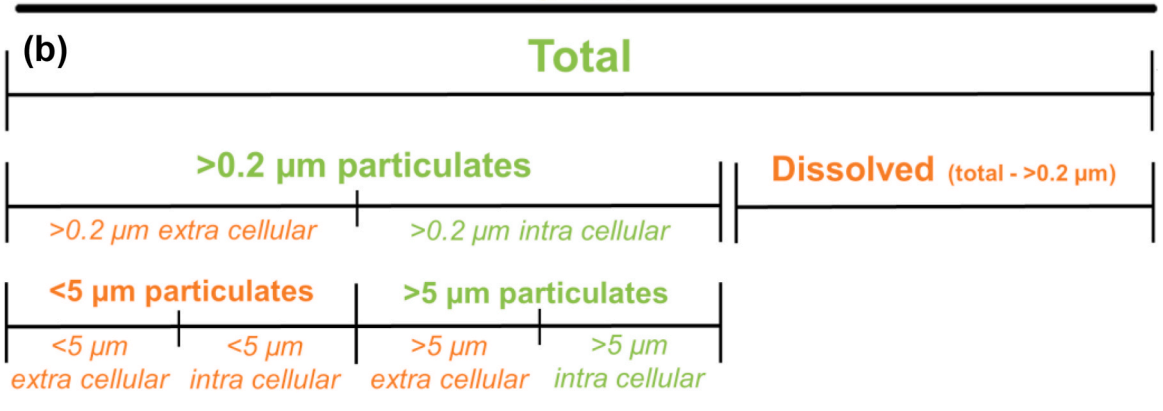

(caption on next page)

Fig. 2. Remineralisation experimental method. (a) Stage 1 uptake measurements by incubating phytoplankton from near surface (18–30 m) water spiked with the radio isotopes ^{14}C, ^{55}Fe and ^{32}Si after Fe limitation has been alleviated to promote uptake which is measured alongside T0 isotope distribution in size fractionated particulates and total fractions for C and Si with the addition of particulate intracellular ^{55}Fe and ^{55}Fe adsorbed to the bottle walls. Stage 2 harvests the particulates that have taken up the radio isotopes and resuspends the >5 μm particulate size fraction in mesopelagic water from 110 m for incubation in the dark. At each time point the radio isotope distribution is measured as per stage 1 with the addition (*) of $DO^{14}C$ and $Di^{14}C$. (b) Measured fractions (green) and calculated fractions (orange) of radio isotope distributions, the <5 μm fraction is calculated as the difference between the >0.2 μm particulates and the >5 μm particulates and applies to both extra and intra cellular. Italic text for intra and extra cellular fractions are for iron only and extra cellular is calculated as the difference between total particulates of that size fraction and intra cellular particulates.

before being stored at room temperature until analysis. Blanks were prepared by filtering 500 mL MilliQ and preparing the filter as described above. Filters were digested in 5 mL of 0.2 M sodium hydroxide solution, incubated at 85 °C for 2 h and subsequently allowed to cool to room temperature. The filters were then neutralised with 0.2 M hydrochloric acid solution. The solution was subsequently analysed using standard colorimetric techniques for silicate analysis using a QuAAtro 39 segmented flow autoanalyser.

Particulate Organic Carbon (POC) samples of 1000 mL of seawater were filtered onto pre-ashed (400 °C, 12 h) Whatman™ GF/F filters (nominal pore-size 0.7 μm, 25 mm diameter). These were then placed in acid-clean Eppendorf tubes, and dried overnight (50 °C) for storage prior to analyses on shore. Blanks were prepared by filtering 1000 mL MilliQ and preparing the filter as described above. On shore, the filters were fumed with 11 M hydrochloric acid for 24 h to remove any inorganic carbon, dried (50 °C, >24 h) and pelleted in tin disks (Elemental microanalysis). The samples were analysed for POC using a *Thermo Fisher* Scientific FLASH 2000 Organic Elemental Analyser.

Hydrographic variables were collected with a *SeaBird SBE 9 plus* SS CTD system.

2.5. Determination of water column trace metal concentrations

Seawater samples were collected from the TM CTD and the OTE bottles were transported into a class-1000 clean air laboratory. Subsamples for dissolved trace metals were gravity filtered through a 0.2 μm membrane cartridge filter (Sartobran-300, *Sartorius*) into 60 or 120 mL acid washed polycarbonate bottles. Separate unfiltered samples were collected for total acid (HCl) dissolvable trace metals (TDTM). All samples were acidified with ultrapure (upa) hydrochloric acid (HCl, *Romil*) under a class-100 laminar flow hood. The concentration of trace metals (Fe, Zn, Mn, Ni, Co, Cu) in total dissolvable and dissolved (dTM) samples was determined using an offline semi-automated pre-concentration standard addition method that has been used previously for seawater samples (without UV oxidation) (Milne et al., 2010) and analysed on a HR-ICP-MS (Rapp et al., 2017).

Briefly, the trace metals in the acidified samples were extracted by loading 15 mL of the sample buffered to within the range of pH 6 to 6.4 with 2 M Ammonium Acetate onto a WAKO (Kagaya et al., 2009) chelate resin column (*Wako Pure Chemical Industries*, Japan), rinsing with 0.05 M Ammonium Acetate (Optima grade, *Romil*) for seawater matrix removal. The sample was then eluted by passing 1.5 mL distilled 1 M HNO_3 over the columns. The resin was then cleaned with the elution acid and preconditioned with 0.05 M Ammonium Acetate for the next sample. Method blanks were determined by taking manifold blanks (contribution of trace metals leached by reagents from valves and pump tubing) and acidified de-ionised water blanks (contribution of trace metals from the upa HCl used for sample acidification). The accuracy of the method was established by repeat quantification of trace metal concentrations of in house reference seawater samples which have been checked for accuracy against inter-calibrated GEOTRACES SAFe reference samples and found to be within the quoted ranges (https://www.geotraces.org/standards-and-reference-materials/; see also Supplementary Table S2). The elution acid containing metals extracted from samples were then run on the HR-ICP-MS (Element II, *Thermofisher*) alongside elution acid blanks and a known multi-element standard to monitor instrument drift. The percentage errors based on the repeat measurements of the in house reference seawater against known values were: Fe, 28% (n = 28); Zn, 21% (n = 10); Mn, 4% (n = 32); Ni, 10% (n = 33); Co, 26% (n = 32); Cu, 6% (n = 33). Limits of detection for trace metals based on 3 x standard deviations of the blanks were: Fe, 0.11 nM; Zn, 0.08 nM; Mn, 0.02 nM; Ni, 0.10 nM; Co, 0.0001 nM; Cu, 0.09 nM. Some surface measurements of Fe at P3A were below the limit of detection with some uncertainty in the accuracy of these surface concentrations.

2.6. Statistical analysis

For the Fe addition bioassay experiments, a one-way analysis of variance (ANOVA) and a post hoc Bonferroni multi comparison test were performed on each time point between the control and Fe amended treatments (chlorophyll-*a* and F_v/F_m measurements). Differences were considered statistically significant at $p < 0.05$.

3. Results

3.1. General oceanography

The deep water P3 study site was within the naturally Fe fertilised HNLC region northwest of South Georgia (Fig. 1). P3 was characterised by a relatively shallow seasonal mixed layer (<70 m; Carvalho et al., this issue) with water temperatures increasing from values during P3A of 2.29 ± 0.14 °C to 3.20 ± 0.28 °C during P3C (Table 1), with a band of colder winter water in the upper mesopelagic (100–200 m) of 0.98 ± 0.19 °C throughout the duration of the cruise. During all occupations, the phytoplankton community in terms of chlorophyll-*a* was dominated by the >10 μm size fraction (Table 1), consisting mainly of large diatoms such as *Fragilariopsis kerguelensis* and *Eucampia antarctica* (Poulton, personal observation). Over the course of the 3 occupations of the site, mixed layer chlorophyll-*a* concentrations decreased from 3.75 ± 1.87 mgm^{-3} during P3A to 1.3 ± 0.32 mgm^{-3} during P3C (Table 1). Mixed layer macronutrient concentrations declined between P3A and P3C; nitrate decreased slightly from 19.38 ± 1.24 μM to 17.61 ± 0.76 μM, while silicic acid declined from 5.03 ± 3.82 μM to 2.28 ± 2.12 μM. Water column variables corresponding to experimental sampling are presented in Fig. S1 in the Supplementary Material.

3.2. Trace metal profiles

Dissolved Fe (dFe) concentrations indicated 'nutrient like' profiles (Bruland et al., 2003), with lower surface (20–40 m) concentrations at all station occupations (Fig. 3a). Surface samples typically had measured dFe concentrations less than 0.10 nM, which are below the limit of detection (0.11 nM) so potentially inaccurate but demonstrate depleted surface concentrations. Dissolved Fe peaks (between 150 and 250 m) were observed within the colder winter water of the mesopelagic, which has presumably accumulated dFe, with higher concentrations (>0.27 nM) below 250 m (Fig. 3a). Acid labile particulate Fe (PFe) (calculated as the difference between the total acid dissolvable and dissolved Fe) follow similar 'nutrient like' profiles as dFe. Acid labile particulate Fe peaked around 160 m depth at P3A and P3B with lower concentrations below this (Fig. 3b). The PFe peaks coincided with the colder water band between 100 and 200 m in the mesopelagic.

Consistent with the dFe profiles, the other measured trace metals

Table 1
Sampling station general oceanographic parameters and timescales. Data from calibrated CTD sensors and from Niskin bottles from the sampling rosette. Bacterial abundance from Rayne et al. (this issue), seasonal mixed layer (Z_{ML}) depth from Carvalho et al. (this issue). Surface data from the top 20 m, dFe, dMn and dZn samples collected from between 20 and 40 m, * denotes concentration below the limit of detection (Fe:0.11 nM) and possible inaccuracy. Upper mesopelagic is taken as 100–300 m (Giering et al., this issue). N/A means not sampled.

Station	P3A	P3B	P3C
Date	15–22 Nov '17	29 Nov – 5 Dec '17	9–15 Dec '17
Latitude (S)	52.40	52.40	52.40
Longitude (W)	40.06	40.06	40.06
Z_{ML} (m)	70	70	60
Surface temperature, °C	2.31–2.48 (n = 44)	2.89–3.38 (n = 52)	3.24–3.62 (n = 27)
Upper mesopelagic temperature, °C (110 m)	0.95–1.46 (n = 10)	0.80–1.22 (n = 12)	0.92–1.12 (n = 6)
Surface dFe (nM)	0.07* (n = 1)	0.17 (n = 1)	0.15 (n = 1)
Surface dMn (nM)	0.04 (n = 1)	0.07 (n = 1)	0.11 (n = 1)
Surface dZn (nM)	0.33 (n = 1)	0.23 (n = 1)	0.85 (n = 1)
Surface Nitrate, NO_3 (μM)	17.96–20.82 (n = 14)	16.71–17.68 (n = 10)	16.80–17.43 (n = 6)
Surface biogenic silica, $bSiO_2$ (μM)	7.18–11.51 (n = 3)	4.98–6.60 (n = 3)	3.43–5.04 (n = 4)
Surface silicic acid, $Si(OH)_4$ (μM)	1.51–8.34 (n = 14)	0.81–0.77 (n = 10)	0.63–1.02 (n = 6)
Surface Particulate Organic Carbon (μM)	20.17–32.15 (n = 5)	15.78–23.57 (n = 3)	14.21–16.58 (n = 4)
Surface $bSiO_2$:POC (mol $^{-1}$)	0.28–0.57 (n = 5)	0.28–0.32 (n = 3)	0.21–0.35 (n = 4)
Surface chlorophyll-*a* (mgm^{-3})	1.14–5.01 (n = 6)	1.59–4.30 (n = 6)	1.18–1.59 (n = 5)
Surface chlorophyll-*a* fraction (mg m^{-3})	0.01–0.03	1.1–0.06	0.04–0.11
>0.2 μm:	0.15–0.36	0.13–0.23	0.13–0.20
>2 μm:	2.93–5.93	1.27–3.44	0.90–1.35
>10 μm	(n = 6)	(n = 6)	(n = 5)
Surface diatom cell abundance (cells mL^{-1})	1319–1855 (n = 3)	502–1812 (n = 3)	279–480 (n = 2)
Surface bacterial abundance, (x10^3 cells mL^{-1})	424–512 (n = 2)	391–639 (n = 2)	639 (n = 1)
Mesopelagic (110 m) bacterial abundance, (x10^3 cells mL^{-1})	N/A	319	N/A

which frequently show surface depletion due to biological uptake displayed 'nutrient-like' (Cu, Zn, Ni) or 'hybrid' (Co, Mn) profiles (Supplementary Fig. S2). Dissolved concentrations were substantially depleted in the surface (20–40 m) layer for all these elements, with values increasing beneath the mixed layer, with peaks at depths >400 m for Cu and Zn, while concentrations decreased below ~150–200 m for the scavenged elements labile Co and Mn. Generally, concentrations of the dissolved trace metals showed little temporal variability, although dFe showed some increases over the three sampling periods, particularly below the mixed layer (Fig. 3a).

3.3. Phytoplankton iron limitation

Measurements of the apparent quantum yield of photochemistry (F_v/F_m) using active chlorophyll fluorescence indicated low values (<0.3) within the bloom (Fig. 4a), as have previously been taken to be indicative of Fe stress (Kolber et al., 1998; Greene et al., 1992; Moore et al., 2005; Nielsdottir et al., 2012). Moreover, measured values of F_v/F_m within Fe-addition experiments indicated significant differences ($p < 0.05$) between the control and Fe amended samples at every time point measured across all four Fe addition experiments. Over the duration of the occupation of the P3 site, both the control and Fe amended samples displayed increasing values of F_v/F_m, potentially indicating a reduction in the extent of *in situ* community Fe stress over time (Fig. 4a).

Chlorophyll-*a* concentrations measured in all Fe addition experiments were also significantly different ($p < 0.05$) between the control and Fe amended samples by the end points of all incubations, with a general decrease in the percentage difference of chlorophyll-*a* between the control and Fe amended samples over the occupation (Fig. 4b). For experiments at P3B and P3C, a significant ($p < 0.05$) increase in chlorophyll-*a* was also detected in the Fe amended samples after just 2 days

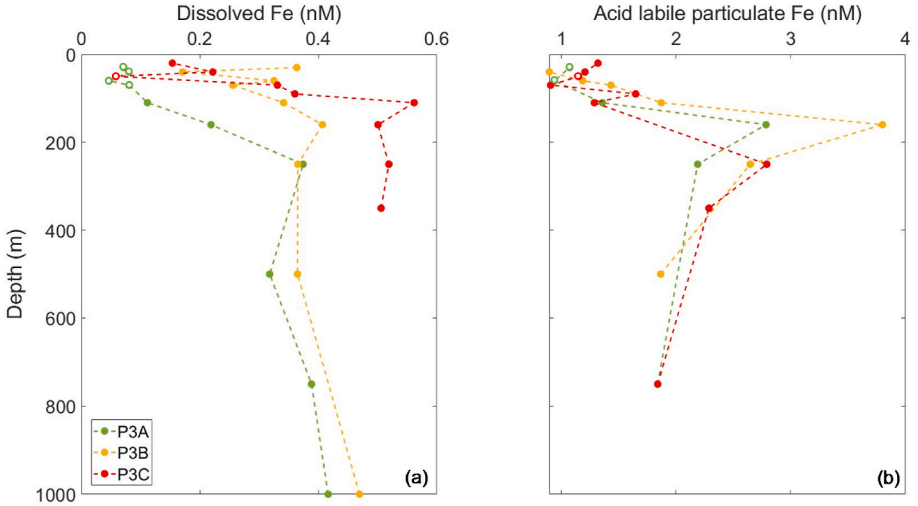

Fig. 3. Iron depth profiles over the P3 occupation: (a) Dissolved Fe, and (b) Acid labile particulate Fe (calculated from total acid dissolvable Fe minus dissolved Fe). Station occupations separated by colour: P3A green line, P3B orange line and P3C red line. Open circles represent data plotted from samples with dFe concentrations less than the 0.11 nM detection limit and hence possibly inaccurate.

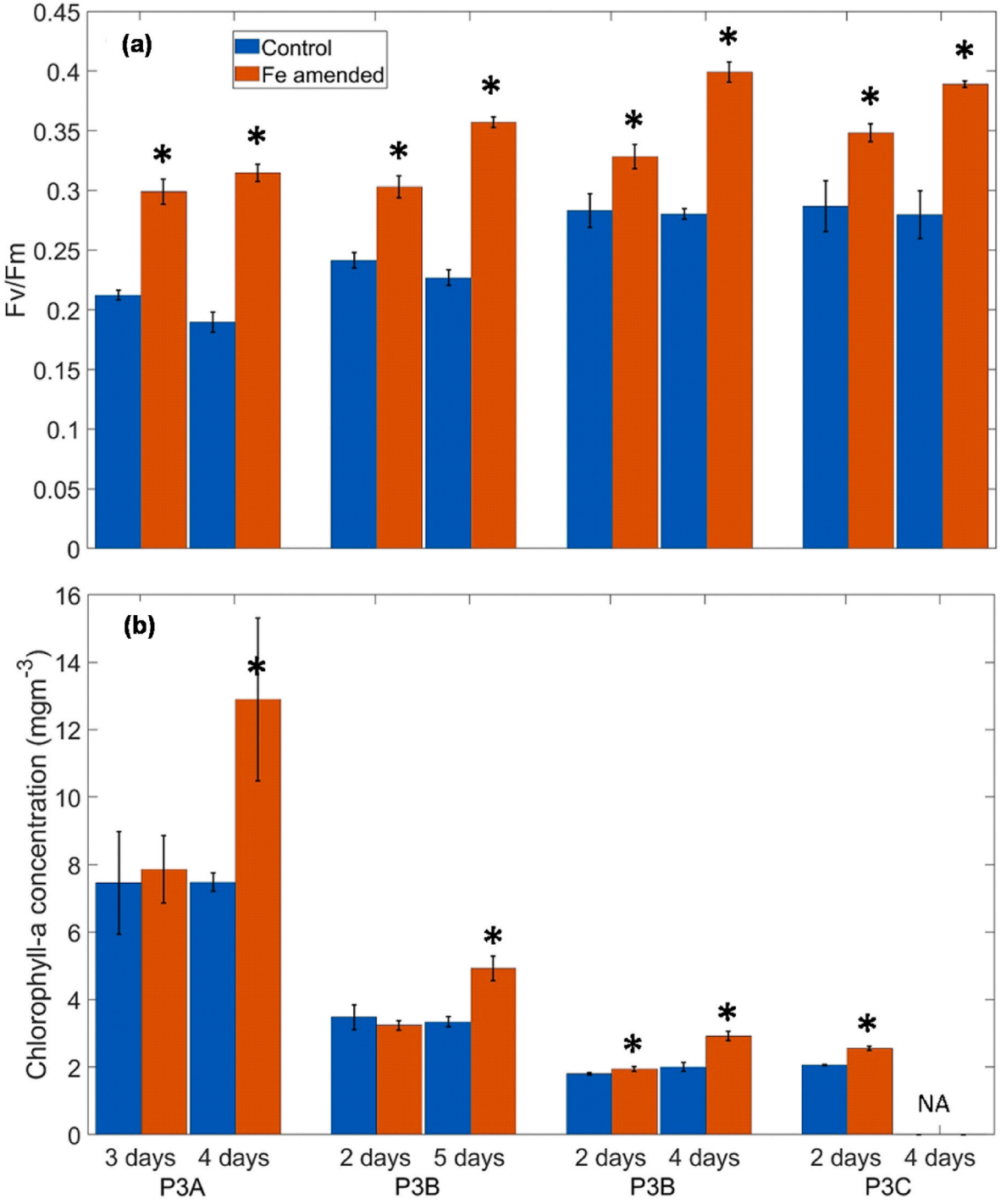

Fig. 4. Phytoplankton Fe limitation responses. (a) Responses of algal physiology to Fe addition; (b) Responses of chlorophyll-a concentrations to Fe addition. In (a) and (b) a significant difference ($p < 0.05$) is indicated by * in the Fe amended samples (red) compared with the control samples (blue). Error bars are shown as 1 standard deviation from triplicate samples. NA indicates not available.

of incubation. Whereas none of the control samples between 2 and 4 days showed any significant ($p < 0.05$) change (Fig. 4b).

3.4. Phytoplankton uptake of Fe, C and Si

Total uptake rates of ^{55}Fe, ^{14}C and ^{32}Si by surface (18–30 m) phytoplankton were calculated after 48 h incubations approximating *in situ* light and temperature conditions (Table 2). Corresponding with the overall decline in upper ocean biomass over the 3 sampling periods, the total ^{14}C uptake decreased over the occupation of P3, from 21 μmol C L^{-1} d^{-1} at P3A to 4.75 μmol C L^{-1} d^{-1} at P3C (Table 2). Total Si uptake similarly indicated a decrease in uptake by the surface phytoplankton over time, from 0.58 μmol Si L^{-1} d^{-1} at P3A to 0.08 μmol Si L^{-1} d^{-1} at P3C (Table 2). The total uptake of ^{55}Fe decreased the least out of the 3 isotopes, from 0.20 nmol Fe L^{-1} d^{-1} at P3A to 0.14 nmol Fe L^{-1} d^{-1} at P3C (Table 2).

Total Si:C uptake ratios ranged from 0.028 mol mol^{-1} during P3A to 0.017 mol mol^{-1} during P3C (Table 2). Ratios of Fe:C uptake ranged from 9.5 μmol mol^{-1} during P3A to 29.5 μmol mol^{-1} during P3C, while ratios of Fe:Si uptake ranged from 0.35 μmol mol^{-1} during P3A to 1.75

Table 2
Average (and Standard Deviation) elemental uptake rates for carbon (C), silica (Si) and iron (Fe), and average stoichiometric ratios. NA indicates not determined.

	P3A		P3B		P3C	
	Total	>5 μm	Total	>5 μm	Total	>5 μm
Uptake rates						
Carbon (C, μmol C L^{-1} d^{-1})	21.00 (5.80)	12.76 (0.71)	8.01 (1.12)	6.70 (1.25)	4.75 (2.06)	3.56 (0.46)
Silica (Si, μmol Si L^{-1} d^{-1})	0.58 (0.15)	0.47 (0.05)	0.03 (0.004)	0.04 (0.01)	0.08 (0.01)	0.07 (0.02)
Iron (Fe, nmol Fe L^{-1} d^{-1})	0.20 (0.04)	NA	0.18 (0.03)	0.12 (0.03)	0.14 (0.007)	0.14 (0.04)
Stoichiometry						
Si:C (mol:mol)	0.028	0.037	0.004	0.006	0.017	0.019
Fe:C (μmol:mol)	9.5	NA	22.5	17.9	29.5	39.3
Fe:Si (μmol:mol)	0.35	NA	6	3	1.75	2

μmol mol^{-1} during P3C. For Si:C uptake ratios, P3B had noticeably lower ratios than during the other sampling time points. In general, stoichiometric uptake ratios for the >5 μm particles were similar to total >0.2 μm particulates for all elements (Table 2).

3.5. Remineralisation experiments

The remineralisation experiments were performed three times, once during each sampling period (P3A, P3B and P3C). Each experiment consisted of 3 timepoints after the stage 2 resuspension, each of these time points were a separate standalone bottle and so represents a pseudo timeseries.

Following stage 1 resuspension of the >5 μm particulates, the activity associated with these particulates becomes the carried over total activity for stage 2. The retention or redistribution of the carried over total activity into size fractionated particulates or the dissolved fraction were then assessed. Comparison of the activity within the carried over total from stage 1 to the retention of activity in the measured particulate (all particulates, >0.2 μm) within stage 2 for ^{14}C were statistically ($p < 0.05$) indistinguishable for all but a single time point. As such, the majority of activity remained in the particulate fraction for 5–6 days in the dark. For ^{32}Si and ^{55}Fe the carried over total and particulates were statistically different ($p < 0.05$) in 30 and 60% of the time points respectively, indicating a measurable dissolved fraction (Fig. 5). In keeping with decreasing biomass (Fig. 1) and decreasing uptake of each isotope from P3A to P3C (Table 2), the particulate activity for ^{14}C and ^{32}Si also decreased whilst ^{55}Fe showed less variability (Fig. 5). The ^{55}Fe data was offset the furthest beneath the 1:1 line indicating greatest measurable dissolved activity (Fig. 5).

3.5.1. Carbon and silica cycling

In most time points (80%), the ^{14}C particulate activity remained within the >5 μm particles, with only a single time point each during P3A and P3B experiments showing a significant ($p < 0.05$) measurement

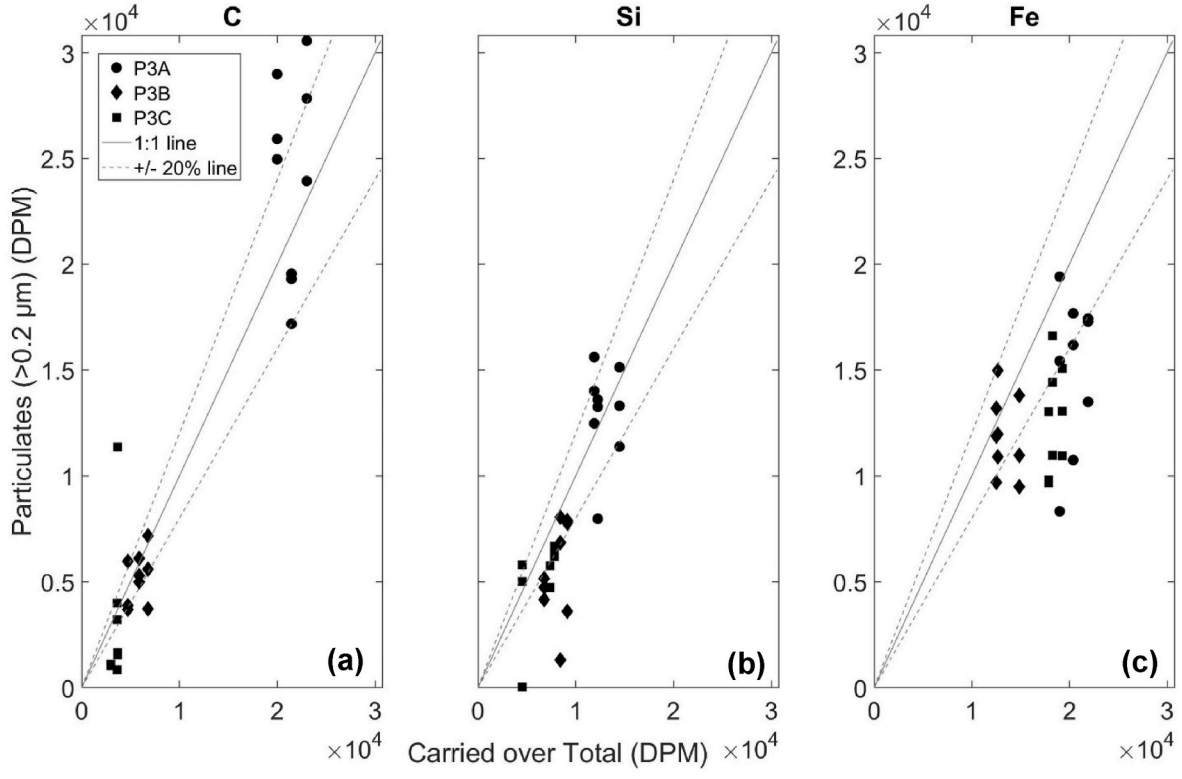

Fig. 5. Carried over total to particulate activity relationship in disintegrations per minute (DPM) for ^{14}C, ^{32}Si and ^{55}Fe in panels a, b and c respectively. Each panel plots all triplicates from each experiment, P3A (circles), P3B (diamonds) and P3C (squares) alongside a 1:1 line (solid grey line) with ±20% offset lines (dashed grey lines). Data points beneath the line represent less activity in the particulate fraction than the carried over total fraction indicating a loss of activity from the particulates into the dissolved fraction.

of ^{14}C in the <5 μm particles. This coupled with only 10% of time points having measurable activity in the dissolved fraction indicates very limited remineralisation of ^{14}C. Acid labile dissolved ^{14}C, assumed to be $DI^{14}C$, was however detected in all time points of all experiments, presumably indicating continued respiration of fixed ^{14}C.

For ^{32}Si, there was also little evidence of remineralisation or dissolution (i.e., movement of ^{32}Si into the smaller particles and/or to the dissolved phase) with 90% of time points showing particulate activity fully retained within the >5 μm particles and only a single time point at P3A resulting in a significant measurement ($p < 0.05$) of ^{32}Si in the small particle fraction (<5 μm). Measurable activity in the dissolved fraction was only detected in 30% of time points.

3.5.2. Iron cycling

Out of the 3 isotopes, ^{55}Fe showed the greatest transfer of activity from the particulates into the dissolved fraction (Fig. 5). Carry over of the ^{55}Fe following resuspension in Stage 2 of the experiments could only come from the particulate material carried across, and so this is the only possible source of ^{55}Fe in the dissolved phase during the subsequent time points.

Following the resuspension of the >5 μm sized particulates, where all of the ^{55}Fe activity was associated with particles (both intra and extracellular) at day 0 (or T0), the subsequent transfer of the ^{55}Fe into smaller particles (potentially due to phytoplankton cell fragmentation and/or remineralisation, microzooplankton or bacterial cell uptake or adsorbtion) or into the seawater (dissolved and adsorbed to the bottle walls) of the sample was assessed. We classify the partitioning of the isotope as being either 'Particle Associated' (PA; ^{55}Fe activity associated either intra and/or extra-cellularly) or 'Seawater' (SW; ^{55}Fe activity either in the dissolved fraction or adsorbed to the bottle walls). Given the extant community was dominated by diatoms throughout our sampling at P3 (section 3.1), we assume that the >5 μm fraction (grown from nutrient addition to the surface (18–30 m) water community), and resuspended into stage 2 of the remineralisation experiments, is also diatom dominated.

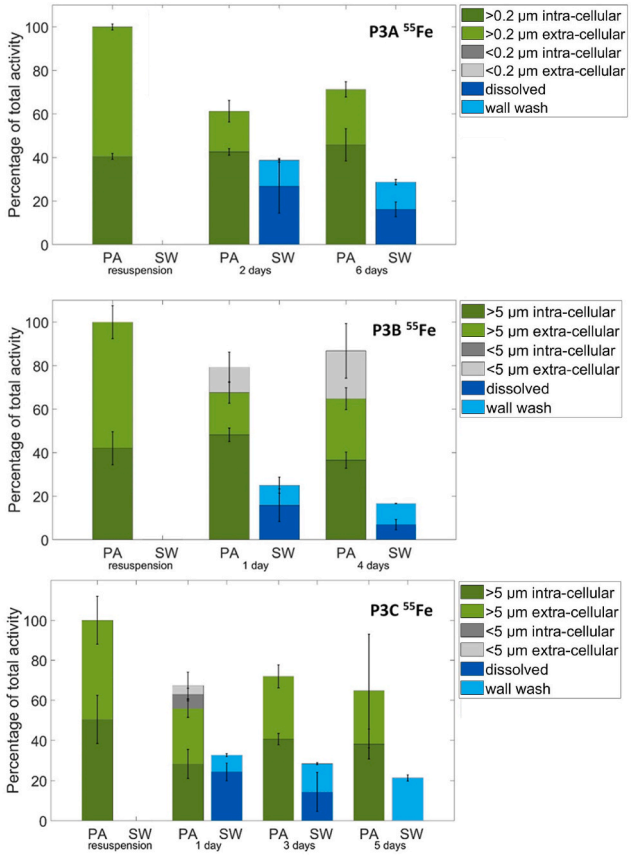

Fig. 6. Relative contribution of each ^{55}Fe fraction to the total activity per time step in each experiment highlighting the presence or absence of ^{55}Fe in the small particulate size fraction and the dissolved phase. PA is particulate associated ^{55}Fe. For P3B and P3C either >5 μm intra-cellular (dark green) or >5 μm extra-cellular (light green), or <5 μm intra-cellular (dark grey) or <5 μm extra-cellular (light grey). For P3A, the size fraction is > 0.2 μm due to no wash performed on the >5 μm fraction. SW is seawater associated ^{55}Fe, dark blue is the dissolved fraction and light blue is the wall wash fraction. Absence of a coloured fraction means that fraction was not significantly ($p < 0.05$) measurable at that time point. Error bars are shown as 1 standard deviation from triplicate samples.

From the first experiment at P3A, the >5 μm resuspended particulates dominated the total (>0.2 μm) particulate pool throughout the experiment (Fig. 6), with no measurable evidence of activity within the <5 μm size fraction particulates at any time point (Fig. 6). Throughout the P3A experiment, the largest proportion of the total activity remained associated with the particles rather than in the seawater (Fig. 6), although 30–40% of the activity was transferred from the PA fraction into the SW fraction.

During P3B, the particulate size fraction was again dominated by the >5 μm particles, however after 1 day and 4 days incubation there was significant ($p < 0.05$) measurable <5 μm particulate activity (Fig. 6). This transfer of ^{55}Fe from the re-suspended large particles to small particles could be as a consequence of cell fragmentation and/or the uptake of isotope by small phytoplankton, heterotrophic flagellates or bacterial cells found in the mesopelagic water used for re-suspension. However, all of the small size fraction associated ^{55}Fe was extracellular, so was adsorbed onto cell surfaces rather than taken up intercellularly. Further, ~20% of total activity was in the seawater fraction after 1 day and 4 days (Fig. 6), again indicating movement of activity off (or out) of the particles.

Consistent with the other experiments, the P3C activity in the >5 μm particles remained dominant at all time points. For P3C, only the first time point (at day 1 post resuspension) showed significant ($p < 0.05$) activity measurable in the <5 μm particulates. This single timepoint indicated the strongest evidence of remineralisation (i.e., a transfer of elements from particle associated to the seawater phase and/or uptake by small particulates) as the measurable activity associated with the <5 μm particules contained non-adsorbed (i.e., potentially intra-cellular) ^{55}Fe contributing to 60% of the <5 μm particle associated ^{55}Fe (Fig. 6). From our results, it is unclear if the small particles were fragments from breakdown of the re-suspended phytoplankton cells or bacterial cells within the resuspension seawater. However, the persistence of both ^{32}Si and ^{14}C within the >5 μm fraction indicates cell fragmentation was likely limited. Within the P3C experiment, there was detectable (~32% of the total activity) transfer of particulate associated ^{55}Fe into the 'seawater', of which 24% was in the dissolved fraction and 8% adsorbed to the walls after 1 day (Fig. 6). While the dissolved proportion decreased (with no measurable dissolved fraction after 5 days), increased ^{55}Fe was scavenged onto the incubation bottle walls (Fig. 6).

3.5.3. Synthesis of remineralisation experiments

Dissolved inorganic ^{14}C was measurable at all time points of all experiments and was likely the main process transferring ^{14}C from the particulate to dissolved fractions. Dissolved ^{32}Si had measurable activity in only 30% of the time points indicating limited loss of Si from the particles. In support of limited evidence of remineralisation of the particles into the dissolved phase, both ^{14}C and ^{32}Si similarly showed only a single time point each of activity in the <5 μm particulate fraction, however it is unknown if the smaller particulates were fragments from the re-suspended phytoplankton or bacterial cells within the whole seawater used for resuspension.

In contrast to both ^{14}C and ^{32}Si, the presence of ^{55}Fe in the 'seawater' fraction was measurable in all experiments at all time points, right from the first sample point post resuspension. In all experiments the dissolved

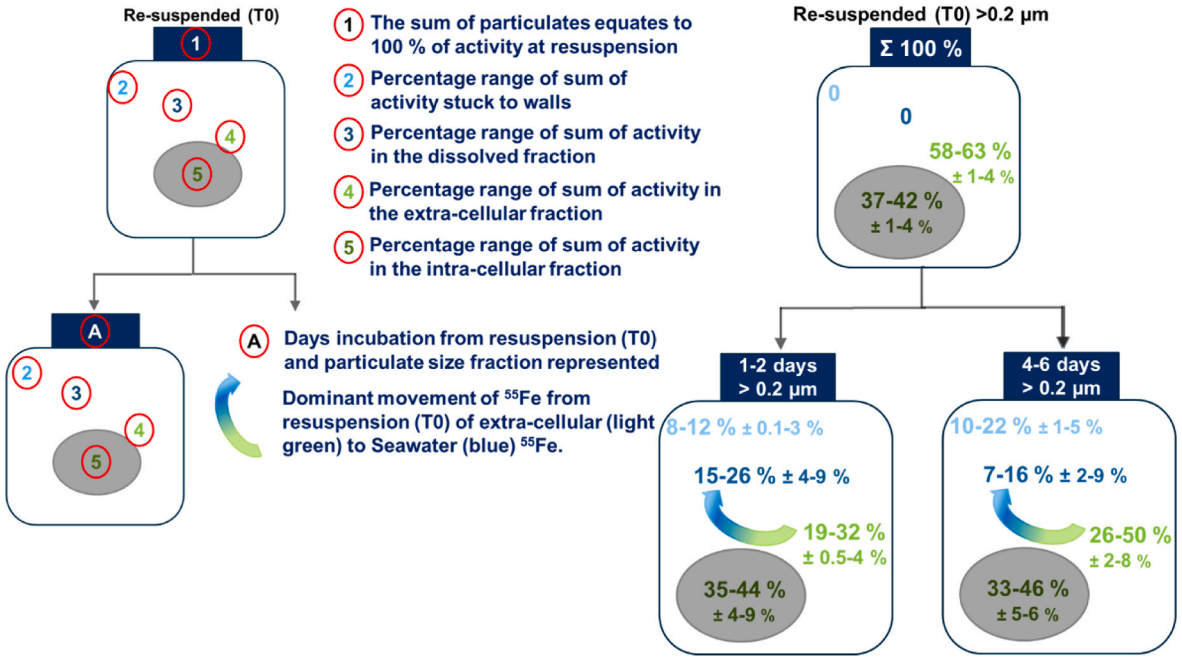

Fig. 7. – Summary plot of all 3 experiments showing ^{55}Fe fractions change from re-suspension into subsequent time points for all particulates (>0.2 µm fraction), showing movement of extracellular ^{55}Fe into the seawater. The top bottle represents the distribution at resuspension (T0) and the bottom bottles represents the distribution of ^{55}Fe at the stated incubation time. Each percentage distribution represents the range from all 3 experiments. All error ranges are 1 standard deviation from triplicate samples.

activity increased to between 7% and 26% of the total activity in the bottle, while the wall wash activity increased by between 8% and 22% (Fig. 7). Moreover, the extra-cellular adsorbed ^{55}Fe on particles decreased from the start of all experiments and timepoints (apart from time point 2 in P3B where the change was insignificant ($p < 0.05$)), dropping from 58 to 63% of the total activity at T0 to 19–50% of the resuspended total activity in subsequent time points (Fig. 7). Given that the non-adsorbed (internal) particle associated ^{55}Fe did not display large changes from resuspension (Fig. 7), the loss of adsorbed ^{55}Fe is the only likely source for the increases observed in ^{55}Fe in the dissolved pool and adhered to the bottle walls. Only a single timepoint measured intra-cellular ^{55}Fe in the small particle fraction (Fig. 6). Presumably, all of the dissolved ^{55}Fe was at least transiently available for uptake by the organisms present, potentially indicating (re)cycling of ^{55}Fe between extra-cellular adsorbed to dissolved phase followed by uptake to become intra-cellular, or direct uptake of adsorbed extra-cellular ^{55}Fe. Following the initial significant ($p < 0.05$) transfer of adsorbed particle associated ^{55}Fe into both seawater associated phases (dissolved or adsorbed to bottle walls), there was no further significant ($p < 0.05$) measurable transfer of ^{55}Fe across subsequent timepoints. This implies that the processes responsible for the transfers observed had broadly reached equilibrium by the time of the first sampling point in all experiments (i.e., after 1–2 days).

Turnover rates for each isotope were calculated by the loss in particulates over time. Carbon-14 averaged a turnover rate of 0.03 d^{-1} (turnover only measurable at a single experiment) and ^{32}Si averaged a turnover rate of 0.030 ± 0.006 d^{-1}, whilst ^{55}Fe turned over at an average rate of 0.06 ± 0.03 d^{-1}.

4. Discussion

4.1. Iron limitation

We sampled the marked annual naturally Fe fertilised phytoplankton bloom north of South Georgia during a decline in chlorophyll and $bSiO_2$ (Table 1) around and shortly after the peak chlorophyll concentration (Fig. 1). Phytoplankton populations within the bloom at P3 were Fe limited during our sampling, as indicated by low (<0.3) absolute values of F_v/F_m and importantly, significantly ($p < 0.05$) increased values rapidly following Fe amendment (Fig. 4a). Development of Fe limitation during the bloom is consistent with previous observations around South Georgia (Nielsdottir et al., 2012; Hinz et al., 2012) and other sub-Antarctic island systems (Moore et al., 2007a&b; Blain et al., 2007). However, Fe stress appears to be less severe later in summer and in autumn within the bloom region (Holeton et al., 2005; Nielsdottir et al., 2012; Hinz et al., 2012).

Surface (20–40 m) dFe concentrations concurrent to the Fe addition experiments were low, ranging from 0.03 to 0.17 nM (Fig. 3, Table 1), indicative of conditions of low Fe bioavailability (<0.5 nM; Johnson et al., 1997). Despite overall low concentrations of Fe (Fig. 3), alongside other bioactive trace metals such as Co, Cu, Ni, Mn and Zn (see Supplementary Material Fig. S2), within surface waters, there was some evidence of increasing near surface concentrations of Fe over the occupations of P3, potentially indicating remineralisation of Fe within and below the diatom bloom. During P3A there was a loss of surface biomass so potentially less Fe demand as the surface community declined (Table 1). Although sub-surface mixing (Blain et al., 2007) could also have contributed to the increased surface concentrations of Fe, no mixed layer deepening was apparent (Table 1), thus any such mixing would have to result from turbulent fluxes across the pycnocline (Blain et al., 2007). Overall, any slight increase in the dissolved Fe pool or supply may reduce Fe stress, as indicated by increasing F_v/F_m from P3B to P3C of 0.35–0.40 (Fig. 4a).

The observed Fe stress, combined with low (<2 µM) upper ocean Silicic acid concentrations may both have been contributing to the decline in bloom intensity following the P3A sampling period (Fig. 1, Table 1). As with other island systems (Planquette et al., 2007), enhanced Fe is likely to accumulate proximal to the islands and shallow sediments around South Georgia in the low light conditions of autumn and winter (Holeton et al., 2005; Nielsdottir et al., 2012). Onset of the bloom in spring would be expected to rapidly deplete Fe and other trace metals (Fig. 3; Supplementary Fig. S2), resulting in the development of Fe stress within an extant population dominated by large celled diatoms (Korb et al., 2010). Diatoms, which dominated the bloom, are lost

through a combination of grazing (Cook et al., this issue) and export (Henson et al., this issue). These loss mechanisms, potentially combined with termination of the increasing phase of the bloom in part due to Fe limitation (Fig. 4) and low Silicic acid (Table 1) will thus contribute to the export of multiple elements, including Fe, from the mixed layer (Boyd et al., 2017).

4.2. Uptake and particulate stoichiometry

The observed Si:C uptake ratios (<0.04 mol mol^{-1}) are low compared to average values for diatoms (0.13 mol mol^{-1}; Brzezinski, 1985). These low values in our experiments are similar to lightly silicified diatom species such as *Chaetoceros* sp. and *Pseudonitzscia* sp. (Brzezinski, 1985), whereas the Si:C ratios for the upper ocean standing stocks indicated heavily silicified cells (0.28–0.57 mol mol^{-1}; Table 1). This discrepancy between low Si:C ratios for uptake relative to high Si:C ratios for the standing stock possibly results from the timing of observations, with decreasing Silicic acid availability (Table 1) and a shift towards lightly silicified diatom species accompanied by export of the more heavily silicified community.

In contrast to C and Si uptake, which can be considered indicative of the ambient conditions due to the tracer concentrations of ^{14}C and ^{32}Si added, measured ^{55}Fe uptake should be considered potential upper bounds as large increases (+2 nM unlabelled Fe and 1.85 nM ^{55}Fe) above the ambient Fe concentrations (0.03–0.17 nM (Fig. 3, Table 1)) are associated with the additions made to the surface (18–30 m) community. Correspondingly, the calculated Fe:C ratios (9.5–29.5 μmol mol^{-1}) thus unsurprisingly fell towards the upper end of observed culture ranges (0.7–70; Strzepek et al., 2012), while also increasing from P3A (Fe:C = 9.5 μmol mol^{-1}) to P3C (Fe:C = 29.5 μmol mol^{-1}) indicating an increase in Fe uptake potential. Although the low dFe concentrations observed during the sampling period (Fig. 3) suggest that these high Fe:C uptake values may not have been reached *in situ*, they do indicate notable potential for rapid biotic Fe accumulation (Schlosser et al., 2018).

Comparing surface mixed layer acid labile PFe concentrations of around 1 nM (Fig. 3) with POC concentrations of around 14–32 μM (Table 1), surface PFe:POC (Fe:C) was around 31–70 μmol mol^{-1} during the sampled stages of the bloom. These ratios were slightly higher than our calculated potential uptake ratios, suggesting a proportion of the acid labile PFe pool may be lithogenic (Schlosser et al., 2018). The observed export of particulate material from the surface during the bloom, combined with shallow C remineralisation (Giering et al., this issue) would thus both have the potential to be notable factors contributing to the observed surface dFe and PFe minima and mesopelagic PFe maxima at depths of ~160 m (Fig. 3), alongside that of other trace metals (Supplementary Fig. S2).

4.3. Remineralisation

The fate of both major (C, Si) and minor (Fe) elements within any exported material will depend on a number of biotic and abiotic processes (Boyd et al., 2017). We thus investigated the potential importance and magnitude of different processes within a series of controlled remineralisation experiments (Fig. 2). The fresh radio-labelled surface (18–30 m) particulates generated within stage 1 of these experiments would have been dominated by diatoms, (section 3.1). Resuspension of this material in mesopelagic water resulted in relatively restricted movements of isotopes between different phases (Figs. 6 and 7). Particles labelled with ^{14}C and ^{32}Si showed little evidence of isotope transfer from particulate into the dissolved phase. In contrast, particles labelled with ^{55}Fe indicated a consistent transfer from the particulate-associated pool into the 'seawater' pool, with this transfer occurring relatively rapidly before the first sampling timepoint (Fig. 6). Since the ^{14}C and ^{32}Si showed little evidence of activity in the dissolved fraction, it is unlikely that the experimental protocol, such as the rinsing step, caused substantial cell rupture and inadvertant transfer of any isotope from the particulate to the dissolved phase.

Some limited accumulation of ^{14}C in the dissolved pool was detected at all time points in the dissolved acid-labile fraction (i.e. ^{14}C labelled dissolved inorganic carbon). It is unlikley that any notable proportion of the ^{14}C labelled dissolved inorganic carbon pool resulted from carryover of the initially added ^{14}C bicarbonate from stage 1, as particulates were rinsed twice with ~50 mL of unlabelled, 0.2 μm filtered mesopelagic seawater prior to re-suspension. Consequently, this pool likely resulted from respiration of (photosynthetically fixed) ^{14}C labelled particulate organic carbon. To determine if the respiration was from the re-suspended diatom dominated surface particulates or from bacteria that may have taken up dissolved organic ^{14}C released from the diatoms and subsequently respired it as DI^{14}C, a parallel experiment was performed at P3B that pre-filtered (0.2 μm) out bacteria from the resuspension water collected from the mesopelagic. The dissolved inorganic ^{14}C results of the filtered (surface >5 μm particulates only) relative to 'whole' (surface particulates and mesopelagic community) samples were not significantly different ($p > 0.05$). This strongly supports the suggestion that the respiration of fixed carbon to aqueous CO_2 (PO^{14}C to DI^{14}C) is from the >5 μm particulates carried over from the first stage of the experiments rather than uptake by mesopelagic bacteria followed by respiration. Evidence of respiration within stage 2 of the experiments indicates that the diatom cells remained metabolically active after being incubated in the dark, and that bacteria mediated remineralisation did not contribute to the respiration signal. Further evidence for the lack of bacterial remineralisation is provided by almost no subsequent appearance of ^{14}C activity in the small particle fraction. Within the parallel ^{32}Si experiments, the small particulate fraction (<5 μm) only had measurable activity for a single time point in one of the three experiments, supporting the evidence of a lack of remineralisation and dissolution of the diatoms. Dissolution of $bSiO_2$ requires bacterial activity to remove the organic matrix before chemical dissolution can act on the $bSiO_2$ (e.g., Bidle and Azam, 1999), which presumably did not occur within our experiments.

Consistent with the results for the major elements C and Si, there was little evidence for bacterial mediated remineralisation for Fe (indicated by isotope activity in small particles), with only a third of all the ^{55}Fe labelled experimental time points having statistically measurable activity in the <5 μm particulates and only one of these time points indicating intra-cellular rather than adsorbed ^{55}Fe. Bacteria might be expected to remineralise small particles faster than large particles (Cavan et al., 2017), so the experiment timeframes with large (>10 μm; Table 1) live diatoms may not have been long enough for the bacteria to break down the particles (cells), despite being more than double the duration of a previous equivalent series of remineralisation experiments (Boyd et al., 2010).

The mesopelagic water for re-suspension from 110 m contained a bacterial abundance of 319 × 10^3 cells mL^{-1} (Rayne et al., this issue; Table 1), whereas a similar experiment that focused on Fe remineralisation by surface (20–40 m) bacteria recorded an abundance of 410–560 × 10^3 cells mL^{-1} and observed rapid (within 72 h) remineralisation of about 40% of the Fe (Boyd et al., 2010). In these previous experiments, the activity in the small size fraction suggested rapid colonisation of the phytoplankton cells by heterotrophic bacteria (Boyd et al., 2010). The slightly higher bacterial abundance in surface waters compared to our mesopelagic abundance could be a contributing factor as to why we observed less transfer of the labelled isotopes into the smaller particulate size fraction. Bidle and Azam (1999) concluded that colonisation intensity rather than overall bacterial abundance had the greatest effect on remineralisation rates. Boyd et al. (2010) and Bidle and Azam (1999) are the only semi-comparable experiments to those we performed, though both showed stronger evidence of remineralisation and differed to our experiments in a number of key ways. The study by Boyd et al. (2010) was dominated by haptophytes whilst ours were dominated by Southern Ocean diatoms. In the case of Bidle and Azam

(1999), various species of diatoms were used, one heavily and one lightly silicified, and the cells were lysed to represent diatom detritus rather than living cells (as in our case and for Boyd et al., 2010). Bidle and Azam (1999) resuspended material in warm waters (16–18 °C) rather than a living community from cold waters as in our experiments (Table 1).

Lack of notable remineralisation in our experiments thus likely resulted from some combination of the relatively short (5–8 day) incubation duration in cold waters, the dominance of the freshly produced particulates by large, live diatoms and potentially low bacterial abundance in the upper mesopelagic. Bacteria have been shown to act on live diatoms (e.g., Passow et al., 2003) in an experiment with a plankton wheel simulating sinking. However, our experimental results are more consistent with *in situ* observations which conclude that large diatoms can sink intact, biologically retaining the micro-nutrients (and the carbon) and increasing the remineralisation length scale of various elements (Twining et al., 2014). Indeed, although relatively short, the 5–8 day duration of our experiments would be comparable to transit times out of the 70 m mixed layer (Carvalho et al., this issue) and through the upper mesopelagic (100–300 m) given even modest sinking rates of 18–60 m d^{-1} for large diatoms (see Villa-Alfageme et al., this issue).

The particulates generated within stage 1 of our experiments were likely dominated by diatoms which were enriched in Fe relative to the Fe limited *in situ* surface community (Fig. 4). Consequently, these organisms might be expected to have an enhanced potential to persist in our simulated dark mesopelagic conditions relative to the *in situ* community. However, measured values of quantum efficiency (F_v/F_m) of photosynthetic cells of sinking material collected in PELAGRA sediment traps (see Giering et al., this issue) were frequently comparable to surface (25–30 m) values for collection depths shallower than 250 m, and on one occasion for a collection depth of 500 m, strongly suggesting that live diatoms were an important export vector *in situ* during our sampling of P3. Consequently, apparent shallow C remineralisation *in situ* within the sampled declining bloom (Giering et al., this issue) must be coupled with processes not captured in our experiments, likely due to a different export vector and/or other processes acting on sinking diatoms within the mesopelagic such as grazing or viral lysis.

4.4. Abiotic release and implications for iron cycling

The most notable transfer of ^{55}Fe we observed was via the (re-) mobilisation of the adsorbed (extra cellular) pool into the dissolved phase (Figs. 6 and 7). This pool comprised over 58% of the total activity carried over from stage 1 in all experiments, but reduced rapidly to less than 50% of the total in the majority of time points and contributed to a significant ($p < 0.05$) measurable increase in the seawater (dissolved and adsorbed to incubation bottle walls) fraction (Fig. 7). Boyd et al. (2010) concluded that rapid colonisation of the phytoplankton cells by heterotrophic bacteria facilitated Fe transfer in their experiments, however they did not distinguish between intra-and extra-cellular associated ^{55}Fe. The mobilisation of adsorbed ^{55}Fe into the non-particle associated phases was key in determining the cycling of Fe in our experiments, as well as our tracking of the ^{55}Fe activity adsorbed to the bottle walls and its consideration as part of the total activity. Adsorbed ^{55}Fe (from the total particulates) present at the point of resuspension was transferred into the dissolved and wall wash fractions by the first time-point in all experiments.

Relating our experiments to *in situ* Fe cycling is complicated by a range of factors. Given the extensive production of organic matter within the bloom, it is likely that biogenic material dominated overall particulate matter both in the surface mixed layer and subsurface. However, *in situ* acid labile Fe:POC ratios suggested that the total PFe pool may have been comprised of a proportion of lithogenic Fe, which may be more prone to scavenging than regeneration (Bressac et al., 2019). Such lithogenic Fe could be a contributing factor to the transfer of mesopelagic Fe from the adsorbed extra cellular pool into the dissolved phase rather than being available for uptake or biological remineralisation (Schlosser et al., 2018). However, it is likely that the majority of the acid (HCl) labile Fe was biogenic.

The (re-)mobilisation of adsorbed Fe we observed in our experiments would be expected to depend on a range of factors, including the concentration and affinity of ligand binding sites of the total particulate pool and in the seawater. The design of our experiments resulted in a ~1:4 dilution of the particulate density between the 1st and 2nd stage (Fig. 2a). Consequently, depending on ligand concentrations and binding strengths in surface mixed layer and mesopelagic waters, it is highly likely that the ligand binding equilibrium was altered between the two experimental stages. Moreover, the 2 nM addition of unlabelled Fe and 1.85 nM ^{55}Fe would mean that dFe concentrations during stage 1 of our experiments would have been higher than those during stage 2, which, in the absence of other changes, would have favoured re-mobilisation of adsorbed Fe. Further, as the particulate (both intracellular and adsorbed) pools of ^{55}Fe dominate the initial condition within stage 2 of our experiments, the ability to resolve abiotic exchange will be biased towards any initial de-adsorbtion, while any subsequent re-adsorption would be difficult to observe, let alone quantify.

Consequently, due to the likely complex kinetic and equilibrium processes involved in (re-)adsorption processes, it is difficult to quantitatively relate the mechanisms we observed in our experiments to those which may be occurring *in situ*. However, given the magnitude of abiotic release, which was on the order of 10–40% of the particulate pool (Fig. 7), such a process could be important *in situ*. For example, if a similar fraction of the acid labile (non-dissolved) Fe concentrations of up to 4 nM in the upper mesopelagic (Fig. 3b), were involved in such a process, this could have a notable impact on the 0.2–0.6 nM dFe pool *in situ* (Fig. 3a). Thus the enhanced observed acid labile particulate and dissolved Fe concentrations (and other trace-metals) within the upper mesopelagic (Fig. 3) suggest that such abiotic processes need to be considered in the context of Fe cycling (Boyd et al., 2017). Specifically, though caution needs to be applied in inferences from repeat observations at a fixed station due to potential advective effects, it is at least conceivable that abiotic release from sinking material, which presumably constitutes at least some of the acid labile PFe (Fig. 3b), could be responsible for a substantial fraction of the apparent increase in sub-surface dFe as the bloom declined and organic material was exported from the surface mixed layer. Similarly, abiotic release from biogenic particles may be important for other elements (Janssen et al., 2021) and may thus influence sub-surface profiles of other biologically active elements (Supplementary Fig. S2). If such a process were indeed notable *in situ*, such rapid (in our case at least <2 days) abiotic release of adsorbed Fe could act to retain this limiting micro-nutrient within the upper mesopelagic, potentially resupplying the surface mixed layer biota and maintaining the bloom through any subsequent mixing into the euphotic zone (Blain et al., 2007; Boyd et al., 2015). Although the reversibility of the (de/re-adsorption) process would again need consideration.

Enhanced dFe concentrations at depth (Fig. 3a) and/or a potentially available adsorbed pool also has potential consequences for the fate of exported material. Any exported live diatoms are likely to be deficient in Fe, as indicated by the low surface (20–40 m) concentrations (Fig. 3) and clear evidence of surface mixed layer Fe limitation (Fig. 4). Access to a sub-surface pool could thus prolong the viability of phytoplankton that have sunk out of the euphotic zone, through replenishing cellular Fe. Hence this could be speculated to increase resistance to remineralisation, increasing C and Si remineralisation length scales, and potentially increasing the chance of these deep diatom populations being mixed back into the upper ocean. Overall, albeit within our experimental context, the (re-)mobilisation of adsorbed Fe resulted in decoupling of C, Si and Fe cycling, with calculated particulate losses corresponding to average turnover rates of 0.06 (±0.03) d^{-1} for ^{55}Fe, which were twice those of ^{14}C or ^{32}Si.

5. Conclusions

We sampled during the peak and post-peak phase of the South Georgia spring bloom, which had reduced surface Fe concentrations and Fe limited phytoplankton. Recycling and mixing of Fe potentially increased the upper ocean dissolved Fe pool, reducing the Fe stress (as indicated by F_v/F_m) of the phytoplankton community. The bloom was diatom dominated, which can act as recognised vectors of Fe export to the deep-sea (Hutchins and Bruland, 1998; Twining et al., 2015). Iron associated with the exterior of the cells (adsorbed extracellularly) may be released as these cells are transferred to depth. Ultimately, the kinetics and equilibrium conditions of such exchange will be influenced by ligand binding site density on cell surfaces of phytoplankton, bacteria and other particulates, as well as in the dissolved ligand pool. However, the magnitude of any such de-absorption at least has the potential to drive substantial differences in the sub-surface dFe concentrations. Given the apparent resistance to degradation, intracellular pools of Fe (along with C and Si) would be expected to be exported to deeper depths with a slower turnover rate if processes such as grazing or cell lysis do not act to break cells up and speed up remineralisation. Our experiments indicate that mesopelagic microbial communities are not the main agents of remineralisation acting directly on sinking healthy, diatom cells. Such a lack of microbe-mediated respiration, dissolution and cell breakdown would tend to increase the remineralisation length scale of the intra-cellular Fe, as well as the C and Si, suggesting that other processes (e.g. zooplankton grazing, viral lysis) are important in driving any shallow remineralisation.

Data calculations and validation

Activity distributions were calculated from both the volumes and the measured activity in the total sample, >0.2 μm particulates, >0.2 μm rinsed (so the intra-cellular biologically retained particles), >5 μm particulates and the >5 μm rinsed sample. The difference between the total in the sample and the total particulate (>0.2 μm extra and intra-cellular) was taken to calculate activity in the dissolved fraction. The particulates were then size partitioned into the smaller size fraction of <5 μm (both intra and extra-cellular) from the difference between the >0.2 μm (i.e. all particles) and the >5 μm particles rinsed and non-rinsed samples. The raw DPM (Disintegrations Per Minute) data (normalised to bottle volume) was validated using the following criteria before individual directly measured or calculated fractions were considered measurable and hence considered in further calculations or results interpretation.

1. The raw DPMs recorded by the scintillation counter should be above the instruments background level of 20 DPM (determined from running a clean filter in scintillation cocktail through the counter). Low raw DPM values could result from the sample volume being too small for the concentration of the isotope to be measurable.
2. The >0.2 μm particulates (i.e. all particles) should have the same or greater DPMs (within 1 standard deviation) than the >5 μm particulates.
3. The non-rinsed particulate samples (^{55}Fe associated both intra and extra-cellular) should have the same or greater DPMs (within 1 standard deviation) as the rinsed particulate samples.
4. The dissolved fraction calculated as the difference between the total DPM and the >0.2 μm particulates DPM was assumed measurable if significantly (*t*-test, $p < 0.05$) greater than zero.
5. The <5 μm particulates fraction calculated as the difference between the >0.2 μm particulates DPM and the >5 μm particulates DPM was assumed measurable if significantly (*t*-test, $p < 0.05$) greater than zero.

Credit author statement

Joanna Ainsworth: Designed the study, performed in field measurements and experiments, processed samples and analysed data, wrote manuscript first draft. Mark Moore and Alex Poulton: Gained funding, designed the study, performed in field measurements and experiments, commented and edited subsequent drafts. Maeve Lohan: Advised on trace metal extractions, commented on drafts. Mark Stinchcombe: Performed field measurements. Alastair Lough: Supported the extraction and processing of the trace metal concentrations, commented on drafts.

Funding

This work was supported by the Natural Environment Research Council grant for the COMICS project. Grant codes: NE/M020835/1, NE/M020835/2, NE/M02072X/1, Studentship (1942696).

Declaration of competing interest

The authors declare that they have no known competing financial interests or personal relationships that could have appeared to influence the work reported in this paper.

Data availability

Data will be made available on request.

Acknowledgements

The authors would like to thank the crew and technicians on the RSS *Discovery* for a very productive cruise, the COMICS project team for providing a very comprehensive dataset, funded by NERC (Natural Environment Research Council) and Hannah East for analysing the POC. The *in situ* chlorophyll time series was collected, calibrated and processed by Nathan Briggs and Filipa Carvalho, funded through a European Research Council Consolidator grant (GOCART, agreement 724416, PI: Stephanie Henson). We would also like to thank Sea Technology Services (STS) for technical assistance with glider deployments, this work was supported by South Africa's Department of Science and Innovation (DST/CON 0182/2017) and the National Research Foundation (SANAP: SNA170522231782). Associated CTD data is available online through the British Oceanographic Data Centre (BODC).

Appendix A. Supplementary data

Supplementary data to this article can be found online at https://doi.org/10.1016/j.dsr2.2023.105269.

References

Atkinson, A., Whitehouse, M.J., Priddle, J., Cripps, G.C., Ward, P., Brandon, M.A., 2001. The pelagic ecosystem of South Georgia, Antarctica. Mar. Ecol. Prog. Ser. 216, 279–308.

Balch, W.M., Drapeau, D.T., Fritz, J.J., 2000. Monsoonal forcing of calcification in the arabian sea. Deep-Sea Res. Part II 47, 1301–1337.

Bidle, K.D., Azam, F., 1999. Accelerated dissolution of diatom silica by marine bacterial assemblages. Nature 397, 508–512.

Blain, S., Quéguiner, B., Armand, L., et al., 2007. Effect of natural iron fertilization on carbon sequestration in the Southern Ocean. Nature 446 (7139), 1070–1074.

Boyd, P.W., 2002. Environmental factors controlling phytoplankton processes in the Southern Ocean. J. Phycol. 38 (5), 844–861.

Boyd, P.W., Jickells, T., Law, C.S., Blain, S., Boyle, E.A., Buesseler, K.O., Coale, K.H., Cullen, J.J., deBaar, H.J.W., Follows, M., Harvey, M., Lancelot, C., Levasseur, M., Owens, N.P.J., Pollard, R., Rivkin, R.B., Sarmiento, J., Schoemann, V., Smetacek, V., Takeda, S., Tsuda, A., Turner, S., Watson, A.J., 2007. Mesoscale iron enrichment experiments 1993–2005: synthesis and future directions. Science 315, 612.

Boyd, P.W., Ibisanmi, E., Sander, S.G., Hunter, K.A., Jackson, G.A., 2010. Remineralization of upper ocean particles: implications for iron biogeochemistry. Limnol. Oceanogr. 55 (3), 1271–1288.

Boyd, P.W., Ellwood, M.J., 2010. The biogeochemical cycle of iron in the ocean. Nat. Geosci. 3, 675–682.

Boyd, P.W., Strzepek, R., Ellwood, M.J., Hutchins, D.A., Nodder, S.D., Twining, B.S., Wilhelm, S.W., 2015. Why are biotic iron pools uniform across high- and low-iron pelagic ecosystems? Global Biogeochem. Cycles 29, 1028–1043.
Boyd, P.W., Ellwood, M.J., Tagliabue, A., Twining, B.S., 2017. Biotic and abiotic retention, recycling and remineralization of metals in the ocean. Nat. Geosci. 10.
Boyd, P.W., Claustre, H., Levy, M., Siegel, D.A., Weber, T., 2019. Multi-faceted particle pumps drive carbon sequestration in the ocean. Nature 568 (7752), 327–335.
Bressac, M., Guieu, C., Ellwood, M.J., Tagliabue, A., Wagener, T., Laurenceau-Cornec, E. C., Whitby, H., Sarthou, G., Boyd, P.W., 2019. Resupply of mesopelagic dissolved iron controlled by particulate iron composition. Nat. Geosci. 12, 995–1000.
Bruland, K.W., Lohan, M.C., 2003. Controls of trace metals in seawater. Treatise on Geochemistry 6, 23–47.
Brzezinski, M.A., 1985. The Si:C:N ratio of marine diatoms: interspecific variability and the effect of some environmental variables. J. Phycol. 21 (3), 347–357.
Cavan, E.L., Trimmer, M., Shelley, F., Sanders, R., 2017. Remineralization of particulate organic carbon in an ocean oxygen minimum zone. Nat. Commun. 8, 14847.
Chisholm, S.W., Morel, F.M.M., 1991. What controls phytoplankton production in nutrient-rich areas of the open sea? Limnol. Oceanogr. 36, 8.
Cole, J.J., Findlay, S., Pace, M.L., 1988. Bacterial production in fresh and saltwater ecosystems: a cross system overview. Mar. Ecol. Prog. Ser. 43, 1–10.
Cutter, G., Andersson, P., Codispoti, L., Croot, P., Francois, R., Lohan, M.C., Obata, H., Rutgers vd Loeff, M., 2010. Sampling and Sample-Handling Protocols for GEOTRACES Cruises.
De Baar, H.J.W., de Jong, J.T.M., Bakker, D.C.E., Löscher, B.M., Veth, C., Bathmann, U., Smetacek, V., 1995. Importance of iron for plankton blooms and carbon dioxide drawdown in the Southern Ocean. Nature 373, 412–415.
Ducklow, H.W., Kirchman, D.L., Quinby, H.L., Carlson, C.A., Dam, H.G., 1993. Stocks and dynamics of bacterioplankton carbon during the spring bloom in the eastern northern Atlantic Ocean. Deep-Sea Res. Part II 40, 245–263.
Eppley, Peterson, 1979. Particulate organic matter flux and planktonic new production in the deep ocean. Nature 282, 677–680.
Goldberg, E.D., 1954. Marine geochemistry 1. Chemical scavengers of the sea. J. Geol. 62 (3), 249–265.
Greene, R.M., Geider, R.J., Kolber, Z., Falkowski, P.G., 1992. Iron-induced changes in light harvesting and photochemical energy-conversion processes in eukaryotic marine-algae. Plant Physiol. 100 (2), 565–575.
Hassler, C., Cabanes, D., Blanco-Ameijeiras, S., Sander, S.G., Benner, R., 2020. Importance of refractory ligands and their photodegradation for iron oceanic inventories and cycling. Mar. Freshw. Res. 71, 311–320.
Hinz, D.J., Nielsdottir, M.C., Korb, R.E., Whitehouse, M.J., Poulton, A.J., Moore, C.M., Achterberg, E.P., Bibby, T.S., 2012. Responses of microplankton community structure to iron addition in the Scotia Sea. Deep-Sea Res. Part II 59–60, 36–46.
Holeton, C.L., Nédélec, F., Sanders, R., Brown, L., Moore, C.M., Stevens, D.P., Heywood, K.J., Stat ham, P.J., Lucas, C.H., 2005. Physiological state of phytoplankton communities in the southwest Atlantic sector of the Southern Ocean, as measured by fast repetition rate fluorometry. Polar Biol. 29, 44–52.
Hudson, R.J.M., Morel, F.M.M., 1989. Distinguishing between extra- and intracellular iron in marine phytoplankton. Limnol. Oceanogr. 34 (6), 1113–1120.
Hutchins, D.A., Bruland, K.W., 1998. Iron-limited diatom growth and Si:N uptake ratios in a coastal upwelling regime. Nature 393, 561–564.
Janssen, D.J., Rickli, J., Abbott, A.N., Ellwood, M.J., Twining, B.S., Ohnemus, D.C., Nasemann, P., Gilliard, D., Jaccard, S.L., 2021. Release from biogenic particles, benthic fluxes, and deep water circulation control Cr and δ^{53}Cr distributions in the ocean interior. Earth Planet Sci. Lett. 574, 117163.
Johnson, K.S., Gordon, R.M., Coale, K.H., 1997. What controls dissolved iron concentrations in the world ocean? Mar. Chem. 57, 137–161.
Kagaya, S., Maeba, E., Inoue, Y., Kamichatani, W., Kajiwara, T., Yanai, H., Saito, M., Tohda, K., 2009. A solid phase extraction using a chelate resin immobilizing carboxymethylated pentaethylenehexamine for separation and preconcentration of trace elements in water samples. Talanta 79, 146–152.
Kolber, Z.S., Prášil, O., Falkowski, P.G., 1998. Measurements of variable chlorophyll fluorescence using fast repetition rate techniques: defining methodology and experimental protocols. Biochim. Biophys. Acta 1367, 88–106.
Korb, R.E., Whitehouse, M.J., Atkinson, A., Thorpe, S.E., 2008. Magnitude and maintenance of the phytoplankton bloom at South Georgia: a naturally iron-replete environment. Mar. Ecol. Prog. Ser. 368, 75–91.
Korb, R.E., Whitehouse, M.J., Gordon, M., Ward, P., Poulton, A.J., 2010. Summer microplankton community structure across the Scotia Sea: implications for biological carbon export. Biogeosciences 7, 343–356.
Kuma, K., Nishioka, J., Matsunaga, K., 1996. Controls on iron(III) hydroxide solubility in seawater: the influence of pH and natural organic chelators. Limnol. Oceanogr. 41, 396–407.
Lamborg, C.H., Buesseler, K.O., Lam, P.J., 2008. Sinking fluxes of minor and trace elements in the North Pacific Ocean measured during the VERTIGO program. Deep Sea Res. Part II Top. Stud. Oceanogr. 55 (14–15), 1564–1577.
Maldonado, M.T., Strzepek, R.F., Sander, S., Boyd, P.W., 2005. Acquisition of iron bound to strong organic complexes, with different Fe binding groups and photochemical reactivities, by plankton communities in Fe-limited subantarctic waters. Global Biogeochem. Cycles 19 (4).
Martin, J.H., 1990. 'Glacial-interglacial CO2 change: the iron hypothesis.'. Paleoceanography 5, 1–13.
Milne, A., Landing, W., Bizimis, M., Morton, P., 2010. Determination of Mn, Fe, Co, Ni, Cu, Zn, Cd and Pb in seawater using high resolution magnetic sector inductively coupled mass spectrometry (HR-ICP-MS). Anal. Chim. Acta 665, 200–207.
Morel, F.M.M., Kustka, A.B., Shaked, Y., 2008. The role of unchelated Fe in the iron nutrition of phytoplankton. Limnol. Oceanogr. 53 (1), 400–404.
Moore, C.M., Lucas, M.I., Sanders, R., Davidson, R., 2005. Basin-scale variability of phytoplankton bio-optical characteristics in relation to bloom state and community structure in the Northeast Atlantic. Deep Sea Res. Oceanogr. Res. Pap. 52 (3), 401–419.
Moore, C.M., Seeyave, S., Hickman, A.E., Allen, J.T., Lucas, M.I., Planquette, H., Pollard, R.T., Poulton, A.J., 2007a. Iron–light interactions during the CROZet natural iron bloom and EXport experiment (CROZEX) I: phytoplankton growth and photophysiology. Deep Sea Res. Part II Top. Stud. Oceanogr. 54 (18–20), 2045–2065.
Moore, C.M., Hickman, A.E., Poulton, A.J., Seeyave, S., Lucas, M.I., 2007b. Iron–light interactions during the CROZet natural iron bloom and EXport experiment (CROZEX): II—taxonomic responses and elemental stoichiometry. Deep Sea Res. Part II Top. Stud. Oceanogr. 54 (18–20), 2066–2084.
Nielsdottir, M.C., Bibby, T.S., Moore, C.M., Hinza, D.J., Sanders, R., Whitehouse, M., Korb, R., Achterberg, E.P., 2012. Seasonal and spatial dynamics of iron availability in the Scotia Sea. Mar. Chem. 30–31, 62–72.
Orsi, A.H., Whitworth III, T., Nowlin Jr., W.D., 1995. On the meridional extent and fronts of the Antarctic Circumpolar Current. Deep Sea Res., Part I 42 (5), 641–673.
Paasche, E., Brutak, S., 1994. Enhanced calcification in the coccolithophorid Emiliania huxleyi (Haptophyceae) under phosphorus limitation. Phycologia 33, 324–330.
Passow, U., Engel, A., Ploug, H., 2003. The role of aggregation for the dissolution of diatom frustules. FEMS (Fed. Eur. Microbiol. Soc.) Microbiol. Ecol. 46, 247–255.
Planquette, H., Statham, P.J., Fones, G.R., Charette, M.A., Moore, C.M., Salter, I., Nédélec, F.H., Taylor, S.L., French, M., Baker, A.R., Mahowald, N., Jickells, T.D., 2007. Dissolved iron in the vicinity of the Crozet islands, Southern Ocean. Deep-Sea Res. part II 18–20, 1999–2019.
Pollard, R., Tréguer, P., Read, J., 2006. Quantifying nutrient supply to the Southern Ocean. J. Geophys. Res. 111, C05011.
Pollard, R., Sanders, R., Lucas, M., Statham, P., 2007. The Crozet natural iron bloom and export experiment (CROZEX). Deep Sea Res., Part II 54 (18–20), 1905–1914.
Pollard, R., Salter, I., Sanders, R., et al., 2009. Southern Ocean deep-water carbon export enhanced by natural iron fertilization. Nature 457, 577–580.
Raiswell, R., Canfield, D.E., 2012. The iron biogeochemical cycle past and present. Geochemical Perspectives 1, 1.
Rapp, I., Schlosser, C., Rusiecka, D., Gledhill, M., Achterberg, E.P., 2017. Automated preconcentration of Fe, Zn, Cu, Ni, Cd, Pb, Co, and Mn in seawater with analysis using high-resolution sector field inductively-coupled plasma mass spectrometry. Anal. Chim. Acta 976, 1–13.
Reuter, J., 1988. Iron stimulation of photosynthesis and nitrogen fixation in anabaena 7120 and trichodesmium (cyanophyceae). J. Phycol. 124, 249–254.
Richier, S., Achterberg, E.P., Dumousseaud, C., Poulton, A.J., Suggett, D.J., Tyrrell, T., Zubkov, M.V., Moore, C.M., 2014. Phytoplankton responses and associated carbon cycling during shipboard carbonate chemistry manipulation experiments conducted around Northwest European shelf seas. Biogeosciences 11, 4733–4752.
Rijkenberg, M.J., Gerringa, L.J.A., Timmermans, K.R., Fischer, A.C., Kroon, K.J., Buma, A.G., Wolterbeek, B.T., de Baar, H.J., 2008. Enhancement of the reactive iron pool by marine diatoms. Mar. Chem. 109, 29–44.
Robinson, J., Popova, E.E., Srokosz, M.A., Yool, A., 2016. A tale of three islands: downstream natural iron fertilization in the Southern Ocean. J. Geophys. Res.: Oceans 121, 3350–3371.
Sanders, R.J., Henson, S.A., Martin, A.P., Anderson, T.R., et al., 2016. Controls over Ocean Mesopelagic interior carbon storage (COMICS): fieldwork, synthesis, and modelling efforts. Front. Mar. Sci. 3, 136.
Schlosser, C., Schmidt, K., Aquilina, A., Homoky, W.B., Castrillejo, M., Mills, R.A., Patey, M.D., Fielding, S., Atkinson, A., Achterberg, E.P., 2018. Mechanisms of dissolved and labile particulate iron supply to shelf waters and phytoplankton blooms off South Georgia, Southern Ocean. Biogeosciences 15, 4973–4993.
Strzepek, R.F., Hunter, K.A., Frew, R.D., Harrison, P.J., Boyd, P.W., 2012. Iron–light interactions differ in Southern Ocean phytoplankton. Limnol. Oceanogr. 57 (4), 1182–1200.
Sunda, W.G., 2012. Feedback interactions between trace metal nutrients and phytoplankton in the ocean. Front. Microbiol. 3, 204.
Tagliabue, A., Sallée, J.-B., Bowie, A.R., Lévy, M., Swart, S., Boyd, P.W., 2014. Surface-water iron supplies in the Southern Ocean sustained by deep winter mixing. Nat. Geosci. 7, 314–320.
Tagliabue, A., Bowie, A.R., DeVries, T., Ellwood, M.J., Landing, W.M., Milne, A., Ohnemus, D.C., Twining, B.S., Boyd, P.W., 2019. The interplay between regeneration and scavenging fluxes drives ocean iron cycling. Nat. Commun. 10, 4960.
Twining, B.S., Baines, S.B., 2013. The trace metal composition of marine phytoplankton. Ann. Rev. Mar. Sci 5, 191–215.
Twining, B.S., Nodder, S.D., King, A.L., Hutchins, D.A., LeCleir, G.R., DeBruyn, J.M., Maas, E.W., Vogt, S., Wilhelm, S.W., Boyd, P.W., 2014. Differential remineralization of major and trace elements in sinking diatom. Limnol. Oceanogr. 59 (3), 689–704.
Twining, B.S., Rauschenberg, S., Morton, P.L., Vogt, S., 2015. Metal contents of phytoplankton and labile particulate material in the North Atlantic Ocean. Prog. Oceanogr. 137, 261–283.